Heliyon 10 (2024) e40662

Contents lists available at ScienceDirect

Heliyon

journal homepage: www.cell.com/heliyon

Research article

Electrochemical and quantum chemical investigation on the adsorption behavior of a schiff base and its metal complex for corrosion protection of mild steel in 15 wt% HCl solution

Badr El-Haitout [a,1], Ratnaningsih Eko Sardjono [b,1], Bouchra Es-Sounni [c], Maryam Chafiq [d,***], Rachid Salghi [a,e,****], Mohamed Bakhouch [f], Aisha H. Al-Moubaraki [g], Jamilah M. Al-Ahmari [g], Azza A. Al-Ghamdi [g], Mohammed Fahim [c], Belkheir Hammouti [e], Abdelkarim Chaouiki [d,*], Young Gun Ko [d,**]

[a] *Laboratory of Applied Chemistry and Environment, ENSA, University Ibn Zohr, PO Box 1136, Agadir, 80000, Morocco*
[b] *Chemistry Program, Universitas Pendidikan Indonesia, Setiabudi 229, Bandung, 40154, Indonesia*
[c] *Laboratory of Innovative Material and Biotechnology of Naturel Resources, Faculty of Sciences of Meknes, Moulay Ismail University, Morocco*
[d] *Integrated Materials Chemistry Laboratory, School of Materials Science and Engineering, Yeungnam University, Gyeongsan, 38541, Republic of Korea*
[e] *Euromed University of Fes, UEMF, Morocco*
[f] *Laboratory of Bioorganic Chemistry, Department of Chemistry, Faculty of Sciences, Chouaïb Doukkali University, P.O. Box 24, El Jadida M-24000, Morocco*
[g] *Department of Chemistry, Faculty of Sciences–Alfaisaliah Campus, University of Jeddah, Jeddah, 21589, Saudi Arabia*

ARTICLE INFO

Keywords:
Corrosion inhibitor
Schiff base metal complex
Electrochemistry
Adsorption behavior
Molecular modelling

ABSTRACT

This work evaluates the effectiveness of Schiff base derivatives, namely, 2,2'-((1E,1′E)-((2,2-dimethylpropane-1,3-diyl)bis(azaneylylidene))bis(methaneylylidene))diphenol (DAMD) and (2-((E)-((3-(((E)-2-hydroxybenzylidene)amino)-2,2dimethylpropyl)imino)methyl)phenoxy) zinc (HDMZ), as corrosion inhibitors for mild steel in a 15 % HCl solution. By employing a blend of experimental assessments and theoretical computations, such as electrochemical tests, morphological observations, and theoretical simulations, the study achieved an impressive up to 94.6 % inhibition efficiency. Notably, HDMZ exhibited significant protective properties. The results of PDP showed that both inhibitors act as mixed-type corrosion inhibitors. SEM surface analysis of the uninhibited and inhibited samples revealed the formation of a protective layer of inhibitor molecules on the mild steel surface to mitigate its corrosion. The Langmuir adsorption model verified the occurrence of dual adsorption, while theoretical simulations offered insights into the underlying interaction mechanisms. The identification of Schiff-based inhibitors reveals a pronounced synergistic effect in corrosion inhibition, marking a significant advancement in

* Corresponding authors.
** Corresponding author.
*** Corresponding authors.
**** Corresponding author. Laboratory of Applied Chemistry and Environment, ENSA, University Ibn Zohr, PO Box 1136, Agadir, 80000, Morocco.
E-mail addresses: maryam.chafiq@yu.ac.kr (M. Chafiq), r.salghi@uiz.ac.ma (R. Salghi), abdelkarim.chaouiki@yu.ac.kr (A. Chaouiki), younggun@ynu.ac.kr (Y.G. Ko).
[1] These authors contributed equally to this work.

https://doi.org/10.1016/j.heliyon.2024.e40662
Received 2 September 2024; Received in revised form 21 October 2024; Accepted 22 November 2024
Available online 23 November 2024

understanding corrosion control mechanisms. This study illuminates the process of forming covalent bonds between inhibitor molecules and iron atoms, presenting a hopeful path towards the advancement of corrosion inhibitors tailored for industrial use. The parallel adsorption configuration and mutual interactions form a stable structure, reinforcing the organic-metal bonds and enhancing both chemical and physical adhesion to the steel surface. These findings indicate that the synergistic effect of molecular interactions and polar-rich regions offers a promising strategy for designing functional hybrid materials.

1. Introduction

In today's dynamic environment, the importance of precise weather predictions cannot be overstated. Similarly, in the oil and gas industry, the prevention of corrosion is of utmost importance. Corrosion can lead to considerable financial losses and safety risks. Due to hydrochloric acid being commonly used in various industrial processes, in the pickling and descaling of metals, oil-well stimulation, and acidizing operations in the gas and oil industry, the inhibition of corrosion in this environment is crucial [1]. For acidification, petroleum industries typically use 15 % HCl solution as it degrades calcium carbonates into water-soluble calcium chlorides. While the acidification process is beneficial during petroleum production, it results in huge economic losses due to corrosion of the oil well's metallic infrastructure. Carbon steel or mild steel is an excellent material for constructing oil well infrastructure (such as downhole tubulars, flow lines, transmission pipelines, etc.). Corrosion of the well infrastructures result in an increase in production costs during the acidification process [2].

As a result, the development of efficient corrosion inhibitors for mild steel in HCl solution is essential to prevent corrosion and ensure the durability and safety of equipment and infrastructure in these industries [3]. However, most existing corrosion inhibitors have limitations such as high cost, environmental concerns, and limited effectiveness [4]. Therefore, there is a pressing need to create novel corrosion inhibitors that are cost-effective, environmentally friendly, and highly effective in inhibiting the mild steel corrosion in HCl solution [5]. The adsorption of organic inhibitors on the surface of mild steel usually occurs through heteroatoms like N, O, and S. These heteroatoms contribute to the formation of a protective film on the metal surface, preventing corrosive species from attacking the metal surface [4].

Various types of organic inhibitors molecules have been synthesized and tested for their corrosion inhibition properties in HCl solutions. Plant-based and synthetic corrosion inhibitors have garnered significant attention among corrosion and protection researchers due to their promising anti-corrosion properties. Tan et al. investigated the corrosion inhibition performance of Pyracantha fortuneana alcohol extracts (PFAE) on copper in H_2SO_4 solution, finding that at a concentration of 600 mg/L, the inhibition efficiency exceeded 95 % [6]. Salim et al. evaluated the inhibitory performance of (E)-1-(5-methylfuran-2-yl)-3-(6-phenylimidazo [2,1-b] thiazol-5-yl)prop-2-en-1-one (MF-PIT) on copper, mild steel, and aluminum in 1 M HCl, achieving an inhibition efficiency of around 97.5 %, 95.9 %, and 92.2 %, respectively, at an optimal concentration of 10^{-4} M [7]. Fellah et al. studied a salicylhydrazone derivative (HBMH) as a corrosion inhibitor for XC38 carbon steel in 1 M HCl, demonstrating a maximum inhibition efficiency of 90 % at 293 K and an inhibitor concentration of 10^{-3} M [8]. Tiwari et al. explored the corrosion inhibition behavior of two thiadiazoline derivatives, DFAT and DIAT, on N80 steel in 15 % HCl, with inhibition efficiencies reaching 96.02 % and 97.05 %, respectively, at just 50 ppm and 303 K [9]. Lastly, Srivastava et al. synthesized a green inhibitor, (E)-2-styryl-1H-benzo[d]imidazole (STBim), for carbon steel in 15 % HCl, achieving an inhibition efficiency of 98 % at a concentration of 200 mg/L [10]. Some of these inhibitors unfortunately have limited effectiveness or pose environmental concerns [11]. However, recent studies have shown promising results for the application of two synthesized organic inhibitors and their role in preventing the corrosion of mild steel in 15 % HCl solution [4,11]. These inhibitors came to substitute traditional inhibitors due to their cost-effectiveness and environmental friendliness, while still providing high corrosion inhibition efficiency [12]. Thus, recent advances in corrosion science have introduced N, S-doped carbon quantum dots (CQDs), which provide efficient, eco-friendly protection against corrosion in acidic environments. These CQDs utilize heteroatoms like nitrogen and sulfur to create strong adsorption layers on metal surfaces, forming protective films that inhibit the ingress of corrosive ions [13]. Similarly, biodegradable inhibitors like pumpkin leaf extract exhibit robust corrosion inhibition by forming stable adsorption films that adhere to the metal surface, even at elevated temperatures [14]. These ligands are used to prepare a wide range of complexes, either mononuclear, binuclear or polynuclear, endowed with divers applications [15,16]. For these reasons, the synthesis of Schiff base and their metal complexes has been of great interest in many fields such as chemistry [17], biology [18–20], and physics [21]. As versatile ligands, Schiff bases are formed by the condensation of primary amines onto carbonyl compounds [22,23]. They have been the subject of many research, due to their ease of preparation and their ability to form metal complexes with almost all metals [24]. Schiff bases are versatile ligands capable of coordinating with metal ions to form stable metal complexes. This flexibility allows for the synthesis of diverse structures with tunable properties by modifying either the Schiff base or the metal ion. Studying the coordination behavior of Schiff bases with various metals provides insight into new bonding interactions, electronic characteristics, and molecular geometries. Consequently, the synthesis of these complexes aims to develop more efficient hybrid materials tailored for specific industrial or environmental applications. Thus, Schiff bases and their metal complexes have been studied as potential corrosion inhibitors [25–29]. In this study, comparing the molecular structures of various inhibitors provides valuable insights into their chemical composition, functional groups, and potential interactions with metal surfaces. Schiff bases and their metal complexes, in particular, emerge as promising candidates for corrosion inhibition due to their aromatic and planar structures, which promote strong adsorption onto steel surfaces. These structural characteristics enhance their interaction with the

metal, making them effective inhibitors. This comparative analysis also helps to clarify structure-activity relationships, offering guidance for the design of more efficient and selective corrosion inhibitors.

On the on the hand, although the importance of experimental studies on the corrosion inhibition properties is undeniable, computational methods have played a pivotal role in understanding mechanisms of inhibiting corrosion and predicting the adsorption behaviors of different inhibitors [30]. At the molecular level and to the best of our knowledge, no previous studies have thoroughly clarified (i) the interfacial interaction mechanisms of the studied inhibitors on metallic surfaces, (ii) the role of various interactions in structural stabilization, and (iii) the driving forces behind the specific spatial rearrangements proposed to develop a robust and stable anti-corrosion system. Thus, we have made every effort to provide a more detailed literature review, place greater emphasis on the novelty of our work, and strengthen the interpretation and discussion of the results. Additionally, we have highlighted the unique contributions of our study within the broader scope of corrosion science and inhibitor development. Thus, quantum chemical calculations, such as density functional theory (DFT), have been employed to investigate the adsorption behavior and electronic properties of organic inhibitors on the steel surface [31]. Moreover, molecular dynamics (MD) simulations can provide valuable insights into the atomic-level interactions between inhibitors and the metal surface [32]. However, the accuracy and reliability of these computational methods are lacking of precision and sometimes can yield conflicting results with experimental findings [33]. Therefore, other methods such as first-principles calculations and density functional tight binding energy calculations have been proposed to overcome these limitations and provide more accurate predictions of corrosion inhibition efficiency. In this paper, the ligand 2,2'-((1E,1′E)-((2,2-dimethylpropane-1,3-diyl)bis(azaneylylidene))bis(methaneylylidene))diphenol (DAMD) as corrosion inhibitor and its corresponding zinc complex, (2-((E)-((3-(((E)-2-hydroxybenzylidene)amino)-2,2dimethylpropyl)imino)methyl)phenoxy) zinc (HDMZ), were synthesized and characterized to investigate their potential as corrosion inhibitors for mild steel in 15 % HCl solution. Anti-corrosion activity of the synthesized Schiff base and its zinc complex were evaluated using weight loss method, electrochemical impedance spectroscopy (EIS) and potentiodynamic polarization (PDP) techniques. The surface morphology of the mild steel samples before and after exposure to the corrosive solution was analyzed using scanning electron microscopy (SEM). To further understand the behavior of the inhibitors, DFT quantum calculations were performed, and MD simulations were carried out to model the inhibitors and mild steel surface interactions. Density functional-based tight-binding (DFTB) technique was used to provide more accurate predictions of interaction energies and what bonds might form between the active sites of the inhibitors and the empty orbitals of iron atoms on the mild steel surface.

2. Method and materials

2.1. Materials and inhibitors

The mild steel samples used in this work were obtained commercially and had a composition of 99 % iron, 0.312 % C, 0.193 % Si, 0.922 % Mn, 0.010 % P, 0.008 % S, and 0.21 % Cr. Specimens for weight loss measurements were prepared by cutting the studied metal into rectangular shapes with dimensions of 1.5 cm × 1.2 cm × 0.4 cm, and polished with progressively finer abrasive papers (from 120 to 2000 grit) to ensure a smooth and clean surface. Then the specimens were cleaned with acetone and deionized water to remove any surface contaminants, and they were allowed to dry at room temperature with air flow. The acidic medium used in this study was a 15 % HCl solution, which was prepared by diluting concentrated commercial 37 % HCl with deionized water. solutions of the synthesized ligand DAMD and its zinc complex HDMZ were prepared in various concentrations, spanning from 10^{-6} to 10^{-3} M in order to evaluate the limits of their corrosion inhibition efficiency [34,35].

2.2. Synthesis of ligand DAMD and its zinc complex HDMZ

All reagents and solvents used were of analytical grade. Chemicals were purchased from Sigma-Aldrich and used as received. AT-IR spectra were recorded on a JASCO FT-IR-4100 spectrometer in the range (400–4000) cm^{-1}. Electronic absorption spectra were recorded in ethanol (10^{-4} M) on a UWR spectrophotometer at room temperature. The element analysis was retrieved with the help of PerkinElmer 2400 Series II CHNS/O elemental analyzer. The melting-point was determined using a Kofler Bench with a precision of ±2 °C.

2.2.1. Synthesis of ligand DAMD

In a 100 mL two necked flask equipped by a condenser, salicylaldehyde (2 mmol, 244.04 mg) was dissolved in ethanol (10 mL). Then, 2,2-dimethylpropan-1,3-diamine (1 mmol, 102.12 mg) dissolved in ethanol (5 mL) was added dropwise through a dropping funnel to the salicylaldehyde and the mixture was refluxed for 1 h. A yellow coloration was observed as soon as the two compounds came into contact. The ethanol was removed under reduced pressure until the formation of a yellow precipitate and cooled in an ace bath. The resulting yellow solid was isolated by filtration and washed with cold ethanol.

Yellow solid; Yield = 94%; m.p. = 57 °C.

RMN 1H ($CDCl_3$, 300 MHz) (δ, ppm): 1.10 (s, 6H, $(CH_3)_2$), 3.51 (d, 4H, $(CH_2)_2$, 4J = 1.07 Hz), 6.91 (dt, 2H, Ar-H, Jm = 1.06 Hz, Jo = 6.47 Hz), 7.00 (d, 2H, Ar-H, J = 8.08 Hz), 7.28 (dd, 2H, Ar-H, Jm = 1.64 Hz, Jo = 7.65 Hz), 7.34 (dt, 2H, Ar-H, Jm = 1.69 Hz, Jo = 8.40 Hz), 8.35 (t, 2H, CH=N, 4J = 1.07 Hz), 13.60 (s, 2H, Ar–OH). RMN 13C ($CDCl_3$, 75 MHz) (δ, ppm): 24.49 ($(CH_3)_2$), 36.26 (C $(CH_3)_2$), 68.13 ($(CH_2)_2$), 117.06, 118.59, 118.74 (C-CH=N), 131.38, 132.65, 161.22 (C-OH), 166.05 (CH=N). IR (KBr) ν (cm^{-1}): 3423

(OH), 1632 (CH=N), 1459, 1496, 1578, 1609 (C=C-C=C), 1278 (C–O). UV–Vis MeOH (λ_{max}, nm, (ε, $M^{-1}cm^{-1}$): π→π*, 257 (15300), 301 (6800); n→π*, 360 (3700); TC 441 (510).

2.2.2. Synthesis of zin complex HDMZ

In a 100 mL boiling flask fitted with a condenser a mixture of ligand DAMD (1 mmol, 310.17 mg), zinc chloride $ZnCl_2$ (1 mmol, 136.28 mg), ethanol (20 ml) and three drops of triethylamine were refluxed under magnetic stirring. The reflux was continued until the consumption of all reagents as evidenced by TLC. Then, the solvent was removed using a rotary evaporator and the obtained precipitate was filtered off, washed with diethyl ether and cold ethanol. The isolated solid was recrystallized in ethanol to give pure HDMZ complex as yellow powder.

Yellow solid; Yield = 76%; m.p > 260 °C.

IR (KBr) ν (cm−1): 1617 (CH=N), 1451 (C=C), 1250 (C–O), 578 (O-Zn), 441 (N-Zn). UV–Vis MeOH (λ_{max}, nm, (ε, $M^{-1}cm^{-}$): π→π*, 256 (12000), 270 (13000); n→π*, 300 (7100); CT 377 (1100). Anal. Calcd for $C_{19}H_{20}N_2O_2Zn$: C, 61.06; H, 5.39; N, 7.50; O, 8.56 %. Found: C, 61.02; H, 5.11; N, 7.39; O, 8.48 %.

2.3. Methods

2.3.1. Weight loss measurements

WL measurements were carried out to assess the corrosion rate of mild steel in 15 % HCl solution with the synthesized Schiff bases DAMD and HDMZ. The polished and pre-weighed mild steel samples were immersed in the 15 % HCl solution containing the synthesized inhibitors for 24h at room temperature [36]. After the immersion period, the samples were carefully removed from the solution, rinsed with deionized water, dried thoroughly and weighted again to quantify the mass loss. All WL measurements were carried out in triplicate for each inhibitor concentration to ensure accuracy and reproducibility of the results. The obtained weight loss results were used to calculate the mild steel corrosion rate in the presence and absence of the synthesized Schiff bases and their inhibition efficiency using the following formulas (equations (1)–(3) [37]:

$$C_R\left(\frac{mm}{year}\right) = \frac{K \times \Delta W}{A \times \rho \times t} \tag{1}$$

$$\eta\ (\%) = \frac{C_R^0 - C_R^{Inh}}{C_R^0} \times 100 \tag{2}$$

$$\theta = \frac{\eta}{100} \tag{3}$$

where, Δ W is the change in weight prior and after immersion in the corrosive solution, A is the surface area of the mild steel sample, t is the immersion time, ρ is the density of mild steel specimen, and C_R^{Inh} and C_R^0 are the corrosion rates of mild steel in the presence and absence of the inhibitors, respectively. While θ theta is the degree of surface coverage by the inhibitors, and η (%) is the inhibition efficiency of the synthesized schiff bases.

2.3.2. Electrochemical tests

Electrochemical experiments were conducted to further evaluate the corrosion inhibition properties of the synthesized Schiff bases, DAMD and HDMZ, on mild steel in 15 % HCl solution. These tests included potentiodynamic polarization curves and electrochemical impedance spectroscopy measurements. A three-electrode electrochemical cell setup was employed, comprising a saturated calomel electrode as the reference electrode, a platinum electrode as the counter electrode, and the mild steel sample serving as the working electrode [38]. The temperature of electrochemical cell was controlled using a thermostat. The PDP curves were obtained by scanning the potential range from −800 mV to −200 mV relative to the open-circuit potential at a scan rate of 1 mV/s. The EIS measurements were conducted over a frequency range of 100 kHz to 10 mHz with a perturbation voltage amplitude of 10 mV. The impedance data obtained were analyzed utilizing equivalent circuit models to extract pertinent electrochemical parameters, including parameters like charge transfer resistance and double layer capacitance. Overall, these electrochemical tests provide valuable information about the effectiveness of the synthesized Schiff bases as corrosion inhibitors by measuring their ability to modify the electrochemical behavior of the mild steel in the corrosive solution. the inhibition efficiencies of the synthesized Schiff bases can be calculated based on the obtained electrochemical parameters using equations (4) and (5) [39]:

$$\eta_{EIS}(\%) = \frac{R_p^{Inh} - R_p^0}{R_p^{Inh}} \times 100 \tag{4}$$

$$\eta_{PDP}(\%) = \frac{i_{corr}^0 - i_{corr}^{Inh}}{i_{corr}^0} \times 100 \tag{5}$$

Where R_p^{inh} and R_p^o are the polarization resistances with and without the presence of the inhibitors, respectively. While i_{corr}^{inh} and i_{corr}^o are

the corrosion current densities in the presence and absence the inhibitors, respectively.

2.3.3. Surface characterization

Surface characterization techniques were employed to analyze the morphology and composition of the MS samples before and after corrosion inhibition using the synthesized Schiff bases. Scanning electron microscopy was applied on the surface of the MS samples that were exposed to 15 % HCl blank solution and inhibited solution with the highest efficiency during 24h. SEM analysis was performed using an FE-SEM appartus (MIRA3 module, TESCAN) equipped with an energy-dispersive X-ray spectroscopy detector, and operating at an accelerating voltage of 15V [40,41].

2.4. Theoretical studies

2.4.1. Quantum chemical calculations

To delve deeper into the inhibition mechanism of the synthesized Schiff bases, density functional theory (DFT) calculations were employed to compute quantum chemical parameters [42]. These calculations involved determining the highest occupied molecular orbital (HOMO) and lowest unoccupied molecular orbital (LUMO) energies, as well as the global reactivity descriptors such as chemical potential, hardness, electronegativity, and electrophilicity index. The Dmol3 package in the Materials Studio software was used for these calculations, employing the B3LYP functional with the 6-31G(d,p) basis set. The COSMO solvent model was used to simulate the effect of the solvent (15 % HCl solution) on the properties of the inhibitors and their electronic structure. The generalized gradient approximation was used to calculate the equilibrium geometries and electronic properties of the molecules. All the calculations were of "fine" quality and were carried and the quantum chemical parameters, such as ΔE_{gap}, IP, EA, X, η, and ΔN were calculated using equations (6)–(11) [43]:

$$\Delta E_{gap} = E_{LUMO} - E_{HOMO} = \mathrm{IP} - \mathrm{EA} \tag{6}$$

$$IP = -E_{HOMO} \tag{7}$$

$$EA = -E_{LUMO} \tag{8}$$

$$\mathrm{X} = \frac{IP + EA}{2} \tag{9}$$

$$\eta = \frac{E_{LUMO} - E_{HOMO}}{2} \tag{10}$$

$$\Delta N = \frac{\Phi_{Fe} - \mathrm{X}_{inh}}{2^{*}(\eta_{inh} + \eta_{Fe})} \tag{11}$$

Considering $\Phi_{Fe} = 4.82$ eV, the total hardness value η_{Fe} for iron was considered as zero.

2.4.2. MD simulations

Molecular dynamics simulations were employed to study the interactions occurred between the synthesized Schiff bases and the MS surface. The simulations were performed using the Materials Studio 6.0 software by BIOVIA with the COMPASS force field. The Forcite module was utilized to generate the initial model of the MS surface by importing the crystal structure of iron and cleave it to the (110) plane. the iron surface constructed with 4 layers that extended to a 5x5 supercell. The simulation box was set to be a cube with periodic boundary conditions in all dimensions and the size was adjusted to ensure that the distance between the iron surface and its surrounding solvent atoms is sufficient to simulate realistic conditions. The simulation box dimensions were (23.56 × 23.56 × 35,65) comprising the iron surface in contact corrosive solution containing 500 water molecules, $10H_3O^{+}$, 10 Cl^{-}, and one of the synthesized Schiff bases. The molecular dynamics simulations were run for a total of 5000 ps using a time step of 1 fs in the NVT form at a temperature of 298 K with "fine" quality [44,45].

2.4.3. First principles DFTB calculations

For a deeper exploration of the electronic structure and binding properties of the synthesized Schiff bases with the MS surface, first principles density functional tight-binding calculations were performed. These calculations allowed us to obtain deep insights into the chemical nature and stability of the interactions between the inhibitors and the MS surface through free energy calculations and density of states analysis. As an outcome of these calculations, we were able to determine and visualize the location and length of the formed bonds between the Schiff base molecules and the MS surface [46–49]. This calculation process was performed using the Slater Koster trans3d functional from the DFTB + code in the Materiel Studio software (version 6.0). The SCC-DFTB approximation was used to manage the Coulombic interactions within the system. The simulations carried out using an 8 × 8 × 8 Monkhorst-Pack k-point mesh to sample the Brillouin zone of the system. The iron surface was modeled the same as in the molecular dynamic simulations [50]. The studies molecules were placed near the iron surface in a planar configuration with a distance of approximately 2 Å from the iron atoms to simulate the inhibitor-Fe complex formation, and replaced inhibitor molecule to 7 Å above the surface to study the projected density of states of both the free inhibitor and the inhibitor-Fe complex. The binding energies were calculated according to equation (12)

bellow:

$$E_{ads} = E_{mol/surface} - \left(E_{surf} + E_{mol}\right) \quad (12)$$

Where E_{ads} is the binding energy between the inhibitor and the MS surface, $E_{mol/surface}$ is the total energy of the system with the inhibitor and mild steel surface, E_{mol} is the energy of the inhibitor molecule alone, and E_{surf} is the energy of the mild steel surface alone.

3. Results and discussion

3.1. Synthesis and characterization of schiff bases compounds

The condensation of 2,2-dimethylpropane-1,3-diamine on two salicylaldehyde molecules leads to the formation of salen ligand DAMD with ONNO chelating sphere. The ligand DAMD is used to prepare its corresponding zinc complex using the method described in our previous research [23]. The obtained complex HDMZ is determined as a mononuclear complex with a tetrahedral geometry (Scheme 1).

The structures of DAMD and HDMZ are established by various analytical methods, namely IR, NMR; UV–Vis, thermal analysis (DTA-TGA) and elemental analysis.

3.1.1. Infrared spectroscopy

The infrared spectrum of the ligand DAMD (Fig. 1) shows a characteristic absorption band for the vibration of the azomethine C=N group at 1632 cm^{-1}, and a band around 3423 cm^{-1} corresponding to the vibration of the phenolic (O-H) bond. Four bands of average intensity can also be observed at 1459 cm^{-1}, 1496 cm^{-1}, 1578 cm^{-1} and 1609 cm^{-1} relating to the vibration of the benzene skeleton (C=C-C=C). The IR spectrum of the complex HDMZ (Fig. 1) reveals the presence of the main vibrational bands' characteristic of the main functional groups. In addition, it indicates the absence of the band related to the vibration of the (O-H) bond, which is evidence of the formation of the (M − O) bond. This formation of the M − O bond is also confirmed by the appearance of new intense bands around 600 cm^{-1}. This confirms the coordination of the ligand with zinc ions by its deprotonation form. The comparison between the ligand and the zinc complex IR spectra indicates that the C=N band undergoes a hypsochromic shift of 10 cm^{-1} in the spectrum of the zinc complex confirming the coordination of the nitrogen atom to zinc ions.

3.1.2. NMR spectroscopy

The ^{1}H NMR spectrum of the free ligand DAMD (Fig. 2), recorded in deuterated chloroform, shows a singlet signal at 13.60 ppm integrating 2 protons corresponding to the protons of the hydroxyl groups (OH) and a triplet at 8.35 ppm integrating 2 protons due to the protons of the azomethine groups (C=N). The spectrum also shows the presence of a singlet signal at 1.10 ppm corresponding to methyl protons and another doublet signal at 3.51 ppm attributable to protons from methylene groups adjacent to the azomethine group (-CH_2-HC=N). The spectrum revealed the absence of the signal between 4 ppm and 6 ppm related to the protons of the two amino groups NH_2.

The ^{13}C NMR spectrum of the DAMD ligand (Fig. 3) shows the presence of signals related to the resonance of all the carbon atoms of the DAMD ligand. A signal at 24.49 ppm attributable to the carbons of the two methyl groups (-CH_3). The signal at 36.26 ppm assigned to the resonance of the aliphatic quaternary carbon. The carbons of the two methylene groups in the position of the azomethine group resonate at 68.13 ppm. The signal located at 166.05 ppm corresponds to the carbon of the azomethine group (C=N). The signals observed at 118.59 ppm and 161.22 ppm are attributable to the two aromatic quaternary carbons linked to the azomethine and hydroxyl groups, respectively.

We have also attempted to perform the 1H and 13C NMR analyses of the Zn complex but we have failed. It is probably due to the paramagnetic property of the obtained Zn complex.

3.1.3. UV–visible

The UV–Vis spectra of DAMD ligand and zinc complex (Fig. 4) were recorded in ethanol solution (10^{-4} M) at 298 K in the range of 200–800 nm. The UV–Vis spectrum of the free ligand DAMD shows the existence of four absorption bands in the range of 257–414 nm, the band located at 257 nm attributed to the π→π* transition involving the localized molecular orbitals of the benzene chromophore. The two bands located at 301 and 360 nm belong to the π→π* and n→π* transitions of the imine chromophore, respectively. And a faint band related to charge transfer transients from the ligand donor atom's bonding orbital to the metal's non-bonding or anti-bonding orbital (LMCT). For the zinc complex, the spectrum exhibits new broad with low-intensity band in the visible range of 500–700 nm attributable to (d-d) transitions of the metal orbitals, which is evidence of the complexation of the ligand with the metal ions.

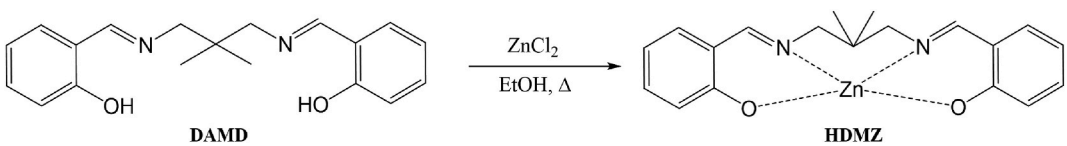

DAMD **HDMZ**

Scheme 1. Synthesis of zinc complex HDMZ.

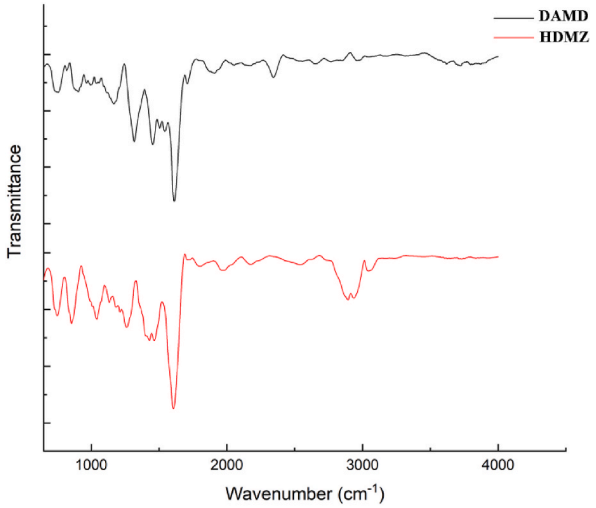

Fig. 1. IR spectra of DAMD and HDMZ.

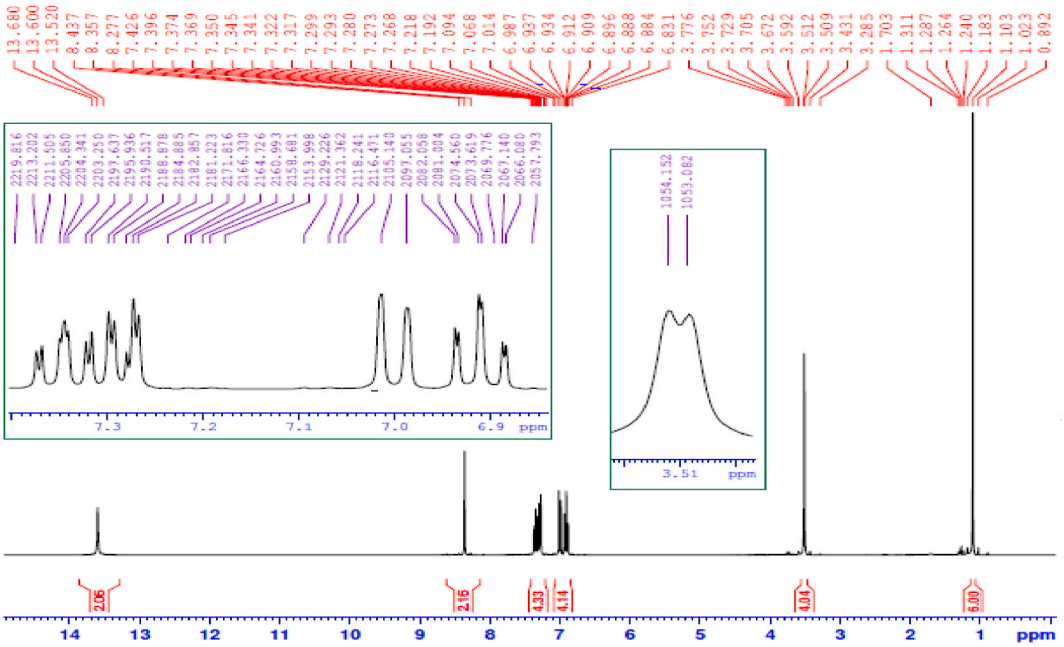

Fig. 2. ^{1}H NMR spectrum of DAMD recorded in $CDCl_3$.

3.1.4. TDA and TGA thermal analysis

The thermal stability of the free ligand DAMD and its zinc complex HDMZ was studied using TGA and TDA methods over a temperature range from room temperature to 1000 °C and illustrated in Fig. 5. The thermograms of the compounds show that the HDMZ zinc complex is stable up to 400 °C, indicating its high stability. However, the ligand DAMD is degrading around 300 °C. A lack of loss relative to the hydrated and complexed water molecules shows that the HDMZ complex is not hydrated.

3.2. Weight loss

WL measurements were performed to evaluate the performance of the synthesized inhibitors (DAMD and HDMZ) in inhibiting the corrosion of MS in 15 % HCl solution at 303 K. The weight loss of the MS coupons without and with different concentrations of the inhibitors was measured after a specific immersion time. Data obtained from the WL measurements were summarized in Table 1 and are presented graphically in Fig. 6. It is observed that both DAMD and HDMZ exhibit excellent corrosion inhibition efficiency, showing a correlation between inhibitor efficiency and their concentration, which increased with higher inhibitor concentrations. At the

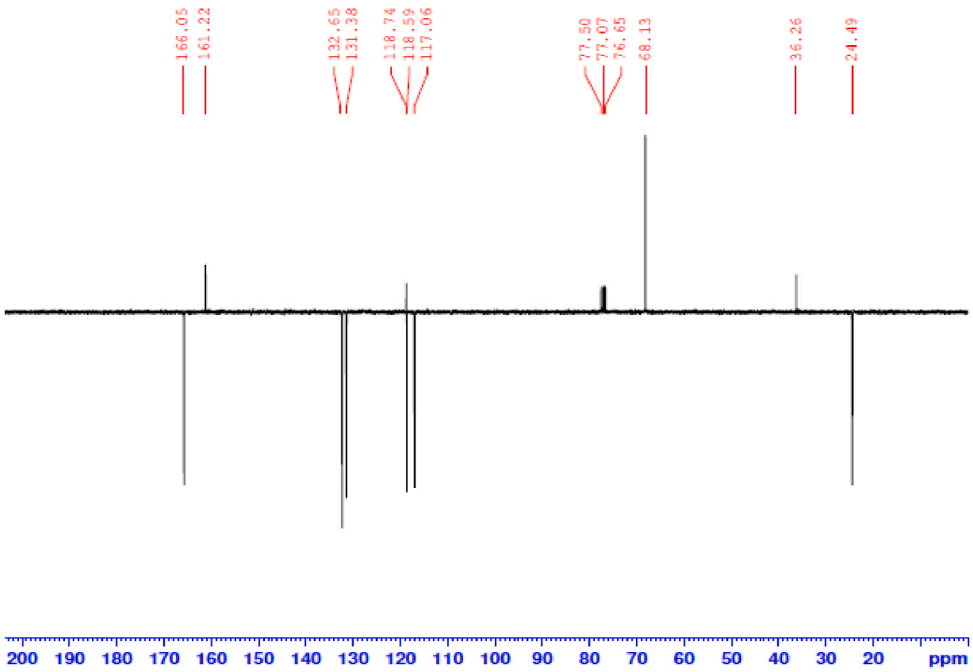

Fig. 3. ^{13}C NMR ($CDCl_3$, APT) spectrum of DAMD.

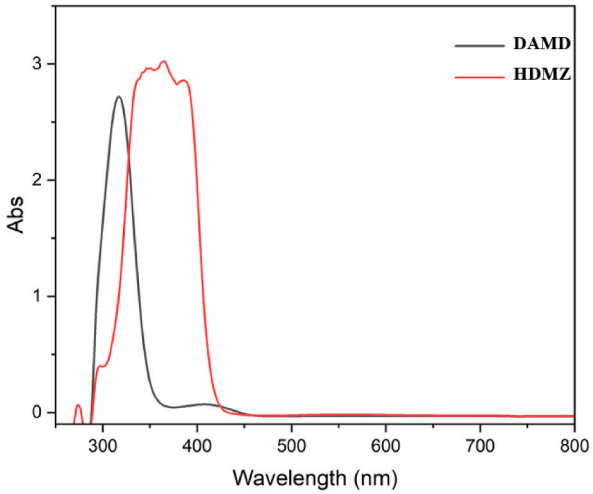

Fig. 4. UV–Vis spectra DAMD and HDMZ.

highest concentration of 10^{-3} M, HDMZ and DAMD achieved inhibition efficiencies of 92 and 89 %, respectively. This increase in inhibition efficiency was accompanied by a decrease in the corrosion rate, which dramatically reduced from 22.15 mm/y in the blank solution to only 2.35 and 1.75 mm/y for DAMD and HDMZ, respectively, at the highest inhibitor concentration. The significant inhibition efficiencies observed for DAMD and HDMZ can be attributed to the adsorption of these inhibitors onto the MS surface. This adsorption facilitates the formation of a protective film, effectively hindering the corrosion process [51].

3.3. PDP measurements

Polarization curves are one of the commonly used electrochemical techniques to evaluate the corrosion behavior of MS in corrosive environments and to comprehend the kinetics of both cathodic and anodic reactions [52]. Data regarding electrochemical parameters including corrosion potential (E_{corr}), corrosion current density (i_{corr}), as well as anodic and cathodic Tafel slopes (βa and βc) are presented in Table 2, along with inhibition efficiency values.

A detailed examination of the polarization curves depicted in Fig. 7 elucidates that both DAMD (Fig. 7a) and HDMZ (Fig. 7b) Tafel

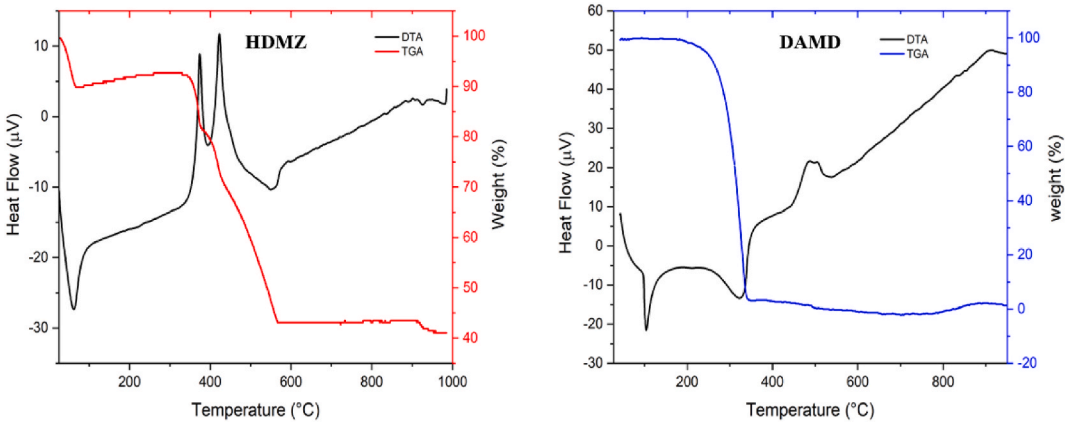

Fig. 5. DTA-TGA thermograms of DAMD and HDMZ complex.

Table 1
Effect of DAMD and HDMZ concentrations on the corrosion data of mild steel in 15 % HCl at 303K

Inhibitor	Concentration (M)	CR (mm/y)	η (%)	Θ
Blank	15 %	22.15	–	–
HDMZ	10^{-3}	1.75	92.12	0.92
	10^{-4}	2.78	87.45	0.87
	10^{-5}	5.47	75.31	0.75
	10^{-6}	8.69	60.78	0.60
DAMD	10^{-3}	2.35	89.41	0.89
	10^{-4}	3.63	83.62	0.83
	10^{-5}	6.61	70.14	0.70
	10^{-6}	10.81	51.21	0.51

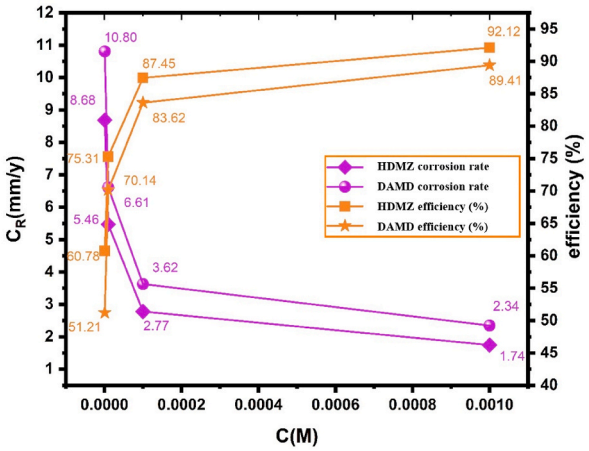

Fig. 6. Variation of corrosion rate and inhibition efficiency, versus inhibitor concentrations of DAMD and HDMZ for mild steel in 15 wt% HCl at 303K

slopes in both anodic and cathodic regions are significantly shifted toward lower values compared to the uninhibited MS, suggesting a reduction in the corrosion current density [53]. This shift implies that the presence of DAMD and HDMZ inhibits both the anodic dissolution of MS and the cathodic reduction of hydrogen ions. In addition, the similarity between the blank and inhibitor-containing solutions in the cathodic branch diagrams indicates that the cathodic reaction mechanism remains unchanged with the presence of DAMD and HDMZ inhibitors [54,55].

The effectiveness of DAMD and HDMZ in inhibiting corrosion can be attributed to their capability to adhere to the surface of mild steel, creating a protective layer. This layer restricts the penetration of corrosive agents onto the metal surface, thereby impeding the corrosion process [56–58]. This appears in the significant decrease in the current density from 1568 μA/cm^2 in the blank solution to

Table 2
Electrochemical parameter values estimated according to PDP curves of mild steel in 15 % HCl solution without and with various concentrations of DAMD and HDMZ at 303K.

Inhibitor	Concentration (M)	$-E_{corr}$ (mV/SCE)	$-\beta_c$ (mV/dec)	β_a (mV/dec)	i_{corr} (μA cm^{-2})	η_{PDP} (%)
Blank	15 %	441	153	102	1568	–
HDMZ	10^{-3}	437	124	75	137	91.26
	10^{-4}	429	120	83	213	86.42
	10^{-5}	449	121	87	317	79.78
	10^{-6}	442	115	79	648	58.67
DAMD	10^{-3}	464	141	81	180	88.52
	10^{-4}	449	107	76	290	81.51
	10^{-5}	438	111	69	453	71.11
	10^{-6}	452	132	71	760	51.53

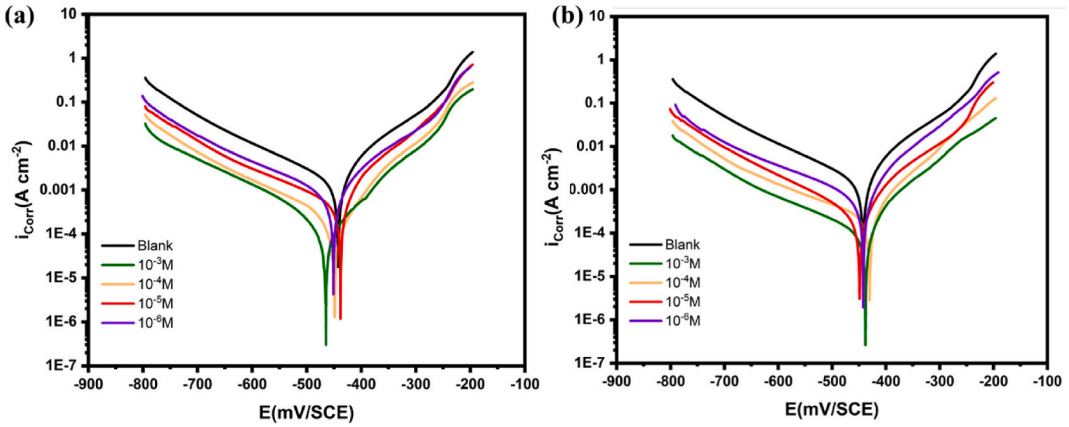

Fig. 7. Tafel plots of mild steel in 15 wt% HCl without and with various concentrations of (a) DAMD and (b) HDMZ at 303 K.

180 and 137 μA/cm^2 for DAMD and HDMZ, respectively, at the highest inhibitor concentration. As a result, a maximum inhibition efficiency of 88 % and 91 % was achieved for DAMD and HDMZ, respectively. On the other hand, as stated by several researchers, the type of inhibition mechanism tested compounds can be deduced from the change in corrosion potential, if it is surpassing ±85 mV, it indicates that the inhibition mechanism is either cathodic or anodic dominant. Otherwise, if the shift in corrosion potential is less than ±85 mV, it indicates a mixed type of inhibition mechanism.

3.4. Electrochemical impedance spectroscopy

Electrochemical impedance spectroscopy technique is one of the simplest yet most effective electrochemical techniques for investigating the corrosion behavior of metals. The EIS technique was utilized to further analyze the corrosion behavior of the mild steel in the presence of the DAMD molecule and its zinc complex HDMZ inhibitors [59–61]. Figs. 9 and **10** depict the Nyquist plots and Bode diagrams, respectively, derived from the EIS measurements conducted on mild steel samples immersed in a 15 % HCl solution, both with and without inhibitors. It can be observed from the Nyquist plots in Fig. 9 that the impedance single arcs are similar in shape

Table 3
Electrochemical parameters values estimated according to EIS curves of mild steel in the presence and absence of several concentrations of DAMD and HDMZ in 15 % HCl at 303 K.

Inhibitor	Concentration (M)	R_s (Ω cm^2)	R_p (Ω cm^2)	n	Q × 10^{-4} (μF/Ωcm^2)	C_{dl} (μF cm^{-2})	η_{EIS} (%)
Blank HCl	15 %	1.51	24.57	0.90	197	96.85	
HDMZ	10^{-3}	1.24	454.6	0.80	11	20.92	94.60
	10^{-4}	1.16	228.1	0.78	17	37.99	89.35
	10^{-5}	2.31	108.8	0.83	24	52.44	77.42
	10^{-6}	1.36	56.94	0.78	27	72.42	56.85
DAMD	10^{-3}	1.13	257.6	0.79	16	34.14	90.44
	10^{-4}	1.12	139.1	0.81	20	39.95	82.45
	10^{-5}	2.07	81.93	0.87	26	44.71	69.67
	10^{-6}	1.45	49.93	0.76	29	82.24	49.86

for the blank solution and the solutions containing DAMD (Fig. 9a) and HDMZ (Fig. 9b) inhibitors, indicating the presence of a consistent corrosion mechanism [62,63]. However, they are different in terms of their diameter, reflecting the variation of the used concentrations, as they get larger while increasing the concentration of inhibitors. This mirrors the EIS parameters summarized in Table 3, which show that the polarization resistance increases with the addition of both DAMD and HDMZ inhibitors in the corrosive environment. At the highest inhibitor concentration, the polarization resistance values for HDMZ and DAMD were 454.6 and 257.6 Ω cm^2, respectively, compared to 24.5 Ω cm^2 for the blank solution. Consequently, a maximum inhibition efficiency of 90 % and 94 % was achieved for DAMD and HDMZ, respectively, as evidenced by the significant decrease in the double layer capacitance from 96.85 μF/cm^2 in the blank solution to 34.14 and 20.92 μF/cm^2 for DAMD and HDMZ, respectively. This behavior also mirrors the findings of Tan et al., where an increase in R_p due to inhibitor adsorption on the metal surface was similarly observed. The protective layer formed by the inhibitors prevents the access of aggressive chloride ions to the steel surface, reducing corrosion [6]. The adsorption of organic inhibitors often leads to the formation of a compact and stable film, reducing corrosion by impeding both anodic and cathodic reactions [64]. It is noteworthy to mention that the double layer capacitance C_{dl} and other EIS parameters such as solution resistance R_s, polarization resistance R_p, and the constant phase element (CPE) parameters (i.e. Q and n) were derived by fitting the experimental data to appropriate equivalent circuit exposed in Fig. 8. The CPE parameters were obtained to accurately represent the behavior of the double layer capacitance. Those parameters were calculated through the impedance of CPE presented by equation (13) [65]:

$$Z_{CPE} = \frac{1}{Q(j\omega)^n} \tag{13}$$

where j is the imaginary unit, ω is the angular frequency, and α represents the fractional exponent.

Using CPE parameters Q and n, polarization and solution resistances R_p and R_s, the double layer capacitance then can be calculated using Brug's formula (eq. (14)) [66]:

$$C_{eff\,dl} = Q_{dl}^{\frac{1}{n}} \times \left(\frac{1}{R_s} + \frac{1}{R_p}\right)^{n-1/n} \tag{14}$$

Moreover, the single capacitive loops in the Nyquist curves indicate the presence of a charge transfer process taking place at the electrode surface. While the depressed Nyquist semicircles suggest the presence of impurities or heterogeneities on the electrode surface [67]. Additionally, Bode phase angle and Bode magnitude plots provide deeper insights into the underlying mechanisms of corrosion and the processes involved in corrosion inhibition, as shown in Fig. 10(a–d). These diagrams illustrate the variation of impedance magnitude and phase angle with the frequency of the applied sinusoidal signal. The impedance magnitude shows a notable increase at lower frequencies for both DAMD (Fig. 10(a and b)) and HDMZ (Fig. 10(c and d)) inhibitors compared to the blank solution, indicating a higher resistance to the corrosion process. This increase in impedance magnitude corresponds to the formation of a protective film due to the adsorption of inhibitors on the MS surface [68]. Furthermore, the phase angle for both inhibitors exhibit a shift towards higher values at lower frequencies, implying a reduction in the rate of corrosion due to inhibition. This shift indicates that the presence of DAMD and HDMZ alters the electrochemical response of MS in the corrosive environment, leading to enhanced corrosion protection.

3.5. *Effect of immersion time on inhibition performance*

The immersion time effect on the inhibition performance of the HDMZ, was investigated through EIS. The impedance measurements were carried out at different immersion times of 0.5, 24, 48, 72, 96, and 120 h to evaluate the prolonged efficacy of the inhibitors in mitigating the corrosion of mild steel within a 15 % HCl solution [69–72]. The Nyquist plots in Fig. 11 display the impedance spectra over the various immersion times. It is observed that the impedance single arcs undergo changes in shape and size with increasing immersion time. The diameter of the arcs decreases with longer immersion times, indicating the variations in the inhibitor's performance over time. The EIS tests reveal that the polarization resistance values for and HDMZ inhibitor show decreasing trend with longer immersion times. Specifically, the polarization resistance values were found to be 454.6, 371.7, 336.6, 212.9, 183.7, and 56.36 Ω cm^2 for immersion times of 0.5, 24, 48, 72, 96, and 120 h, respectively. The findings suggest that the inhibition efficiency of HDMZ

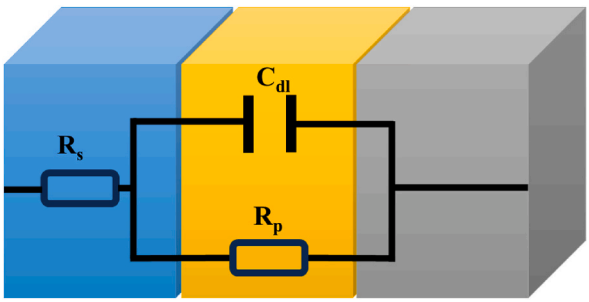

Fig. 8. Electrical equivalent circuit used to fit EIS data.

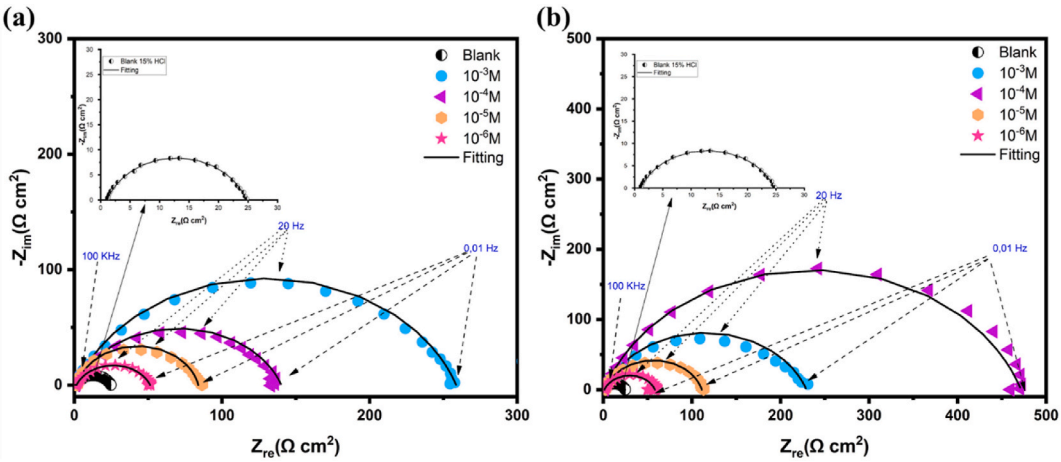

Fig. 9. Nyquist diagrams for mild steel corrosion in 15 wt% HCl with and without various concentrations of (a) DAMD and (b) HDMZ inhibitors.

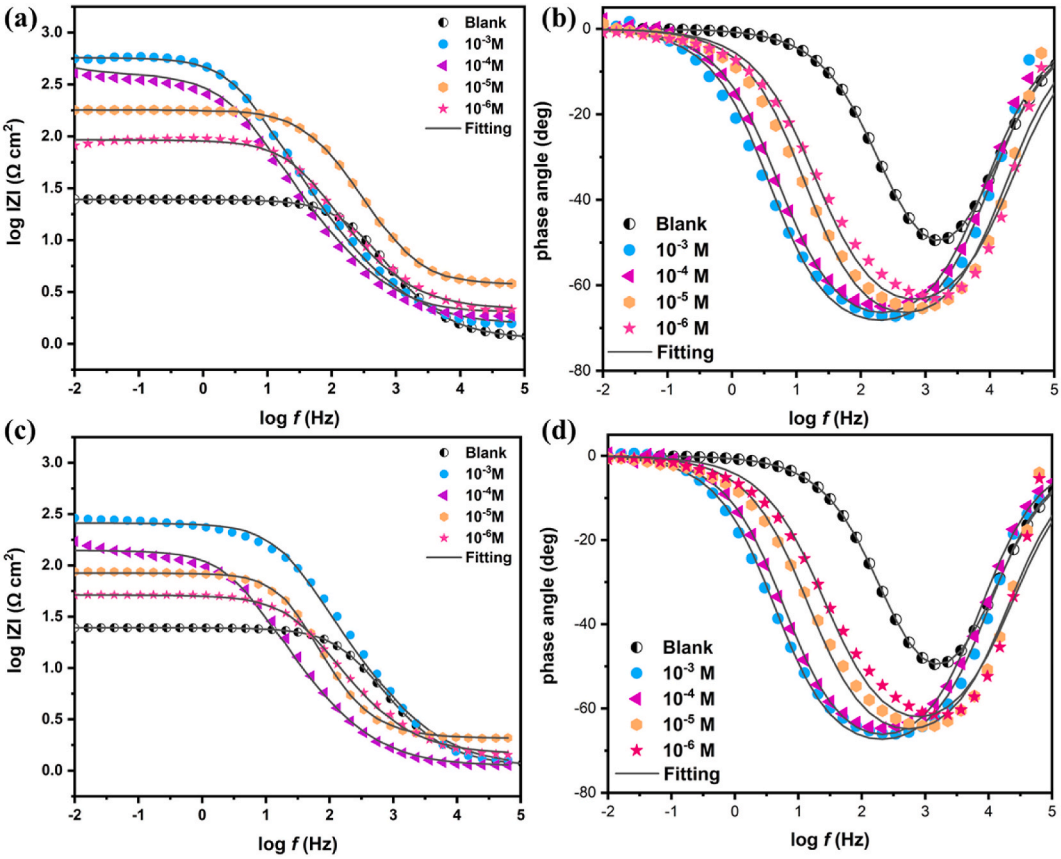

Fig. 10. Bode diagrams of corrosion behavior for mild steel in 15 wt% HCl with and without various inhibitor concentrations: (a, b) HDMZ and (c, d) DAMD.

inhibitor is influenced by the duration of immersion, with decreased performance over the investigated time frame. The investigation of immersion time regarding inhibition performance offers significant insights into the time-dependent behavior of the synthesized inhibitors, shedding light on their potential for sustained corrosion protection in industrial settings. Further studies to explore the inhibitors' performance under varying environmental conditions and exposure durations would contribute to a comprehensive understanding of their practical applicability [73–76].

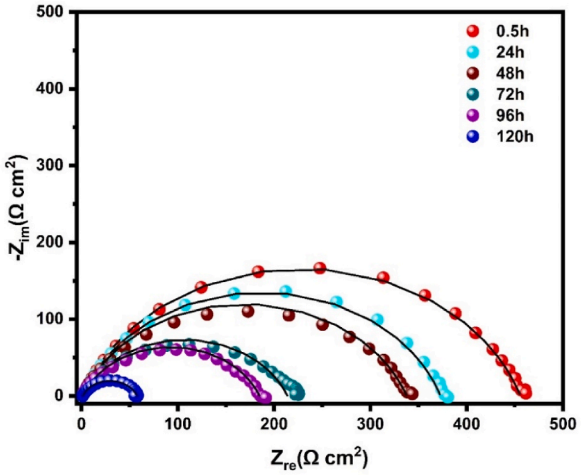

Fig. 11. (a) Nyquist curves for mild steel in 15 wt% HCl with the optimum concentration 10^{-3} M of HDMZ during various periods of immersion.

3.6. Adsorption isotherm

The previous gravimetric and electrochemical tests indicated that the steel's metallic structure was protected from dissolution by the formation of an inhibitive monolayer on the MS surface. However, the thermodynamic mechanism through which this occurred is still not fully understood. To shed light on this area, several models have been created and used to investigate the adsorption process of inhibitors on the MS surface. These models include Flory-Huggins, Freundlich, Temkin, Frumkin, and Langmuir [77–80]. The Langmuir model, in particular, has been frequently used by scientists due to its detailed explanatory approach, making it a suitable model to adopt [81–83]. This model provides a comprehensive understanding of the adsorption process of inhibitors on the MS surface, offering valuable insights into the inhibition performance. It is also characterized by its correlation between the surface coverage parameter and the inhibitor concentration, expressed by equation (15) [84]:

$$\frac{C_{inh}}{\theta} = \frac{1}{K_{ads}} + C_{inh} \tag{15}$$

where C_{inh} represents the inhibitor concentration, θ represents the surface coverage of the inhibitor on the steel surface, and K_{ads} is the adsorption equilibrium constant. Plotting C_{inh}/θ against C_{inh} results in straight lines, as shown in Fig. 12, and Table 4 provides a list of the important linear regression parameters.

The K_{ads} high values presented for both DAMD and HDMZ inhibitors indicate a favorable adsorption process on the mild steel surface [85]. The free energy of adsorption ΔG^0_{ads} is another important parameter that can be calculated using the K_{ads} value obtained from the Langmuir isotherm model through equation (16) [86]:

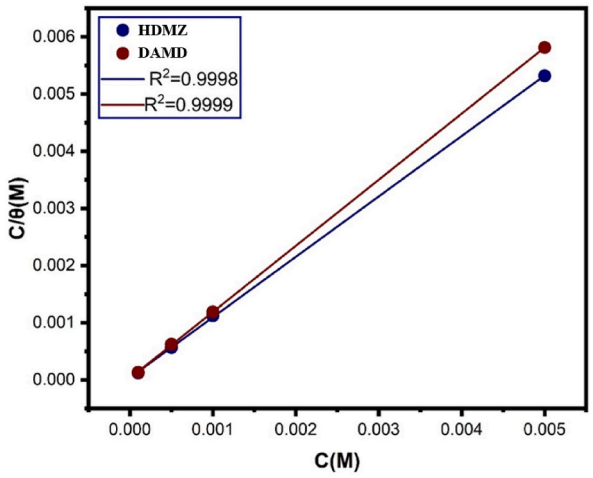

Fig. 12. Langmuir adsorption isotherm fitted to experimental data from weight loss tests.

Table 4
Adsorption descriptions for the corrosion of mild steel in presence of both compounds at 303 K.

Inhibitor	Slope	K_{ads} (M^{-1})	ΔG°_{ads} (KJ/mol)
HDMZ	1,0731	63347	−38.581
DAMD	1,1131	52632	−38.106

$$\Delta G^{0}_{\text{ads}} = -\text{RTln}(55.5 \times K_{\text{ads}}) \quad (16)$$

Where R = 8.314 J K^{-1} mol^{-1}, T = 303 K, and 55.5 mol/L is the concentration of water in the metal/solution interface.

The next step is to predict the adsorption process that might occur based on the calculated ΔG^{o}_{ads} value. According to literature, the adsorption mechanisms are categorized as physical, chemical, or mixed type (physicochemical) [87]. The ΔG^{o}_{ads} parameter obtained for both DAMD and HDMZ inhibitors lies in the range of −20 kJ/mol to −40 kJ/mol. As per literature, if the ΔG^{o}_{ads} value is in this range, it indicates a mixed type adsorption process, a combination of both physical and chemical adsorption mechanisms taking place on the mild steel surface[88–90]. This mixed type adsorption mechanism signifies that the inhibitors exhibit characteristics of both physical and chemical adsorption on the mild steel surface [91,92]. Understanding these adsorption mechanisms is crucial for evaluating the long-term performance and practical effectiveness of the inhibitors in real-world applications. Further exploration of the adsorption process using characterization and computational methods is essential to gain comprehensive insights into the inhibitors' behavior and practical applicability. This will facilitate a more profound comprehension of the interplay between physical and chemical adsorption mechanisms, providing valuable information for potential industrial use.

3.7. SEM observations

In addition to the electrochemical and adsorption studies, SEM observations were performed out to visually assess the surface morphology of the steel samples under different conditions. The pre-prepared steel specimens were immersed for 24 h in acidic solutions without and with the presence of 10^{-3} M HDMZ [93,94]. Fig. 13 illustrates the SEM images of the uninhibited and inhibited surface morphology of the studied samples [80]. Fig. 13a clearly shows the extent of damage that occurred on the metallic surface in the blank solution, attributed to the aggressive nature of the 15 % HCl solution. In contrast, the inhibited sample displayed in Fig. 13b exhibits a remarkable change in surface morphology, manifesting a smooth surface with minimal destruction. This considerable improvement is a result of the central role of the novel Schiff-base compounds in retarding the corrosion rate by adsorbing onto the steel surface, effectively separating it from the corrosive media. The SEM observations complement the findings from the electrochemical and adsorption studies, providing visual evidence of the protective effect of the inhibitors on the steel surface. This comprehensive assessment further reinforces the potential practical applicability of the synthesized inhibitors in the corrosion protection [95,96].

3.8. COSMO-RS sigma-profile analysis

COSMO-RS (conductor-like screening model for real solvents) stands as a computational tool of considerable importance for unraveling the solvation tendencies of molecules. It enables researchers to grasp complex molecular interactions within solvents [97,98]. During the investigation of DAMD and HDMZ, the utilization of COSMO-RS provided significant insights into their solvation characteristics. Fig. 14 depicts the sigma profiles of these molecules, unveiling a nuanced interaction within the solvent environment. Upon closer inspection of Fig. 14, it becomes apparent that DAMD and HDMZ molecules exhibit a complex sigma profile, distinct from that of water. Peaks are observed in both the hydrogen bond donor and acceptor domains, signifying the polar nature of these

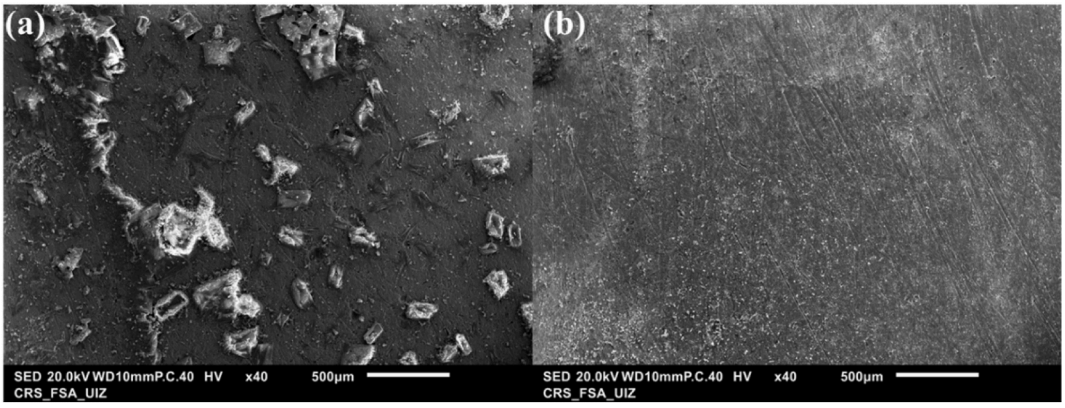

Fig. 13. SEM images of mild steel in (a) 15 wt% HCl and (b) inhibited with 10^{-3} M of HDMZ after 24 immersion time.

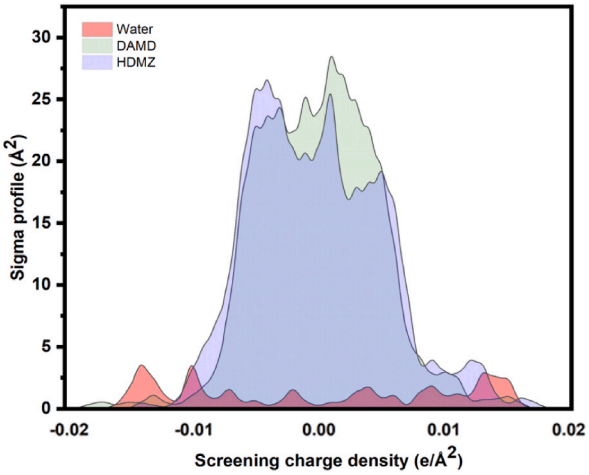

Fig. 14. Calculated sigma-profiles of DAMD and HDMZ molecules using COSMO-RS model at DFT/GGA level.

molecules. These peaks suggest a tendency for these molecules to establish connections with water molecules via hydrogen bonds. Such bonding dynamics can profoundly impact the solubility of these organic molecules, implying a heightened propensity for enhanced solubility [97,98].

3.9. Theoretical results

3.9.1. Global and local reactivity results

Drawing upon existing literature, this approach has allowed researchers to analyze the overall reactivity of inhibitor molecules belonging to diverse organic families, including hydrazones, carboxylic acids, ketones, and amines [99–101]. Typically, these molecules are employed to prevent the corrosion of MS in acidic environments like HCl, HF, and H_2SO_4. In our study, we utilized DFT to enhance our comprehension of the reactivity of two specific molecules (DAMD and HDMZ) in inhibiting MS corrosion within a 15 % HCl acidic medium. We contend that DFT serves as a suitable method for assessing the reactivity of molecules within this family and is well-suited for preventing MS corrosion in acidic environments. Furthermore, we posit that DFT is an effective tool for evaluating both the global and local reactivity of these molecules [102,103]. Fig. 15 provides a schematic representation of the optimized molecular orbital structure, illustrating the most occupied (HOMO) and least occupied (LUMO) molecular orbitals. Additionally, various

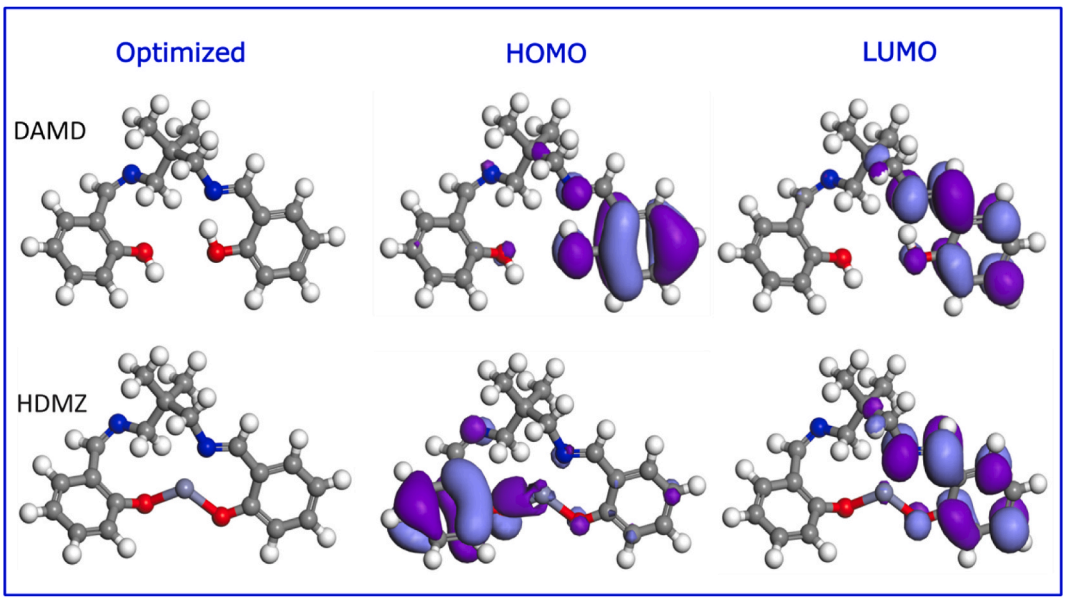

Fig. 15. Optimized geometry, LUMO, and HOMO of the inhibitor molecules DAMD and HDMZ. DFT/GGA theoretical models were used to determine these properties.

theoretical chemical parameters were calculated in the study, including HOMO energy (E_{HOMO}), LUMO energy (E_{LUMO}), gap energy (ΔE_{gap}), electronegativity (χ_{inh}), and transfer electrons (ΔN_{inh}). These findings are detailed in Table 5.

As depicted in Fig. 15, the HOMO and LUMO isosurfaces exhibit a uniform distribution over the phenyl ring and heteroatoms of both inhibitor molecules, DAMD and HDMZ. This uniformity signifies that these specific sites serve as active adsorption sites on the MS surface, indicating the molecules' capacity to accept electrons from donor substances [104–106]. Examining Tables 5 and it is clear that both inhibitors possess elevated HOMO energies and low LUMO energies, suggesting facile electron transfer between the molecules and the MS surface. These findings are corroborated by the electron transfer results, all exceeding 0, signifying an enhancement in the molecules' affinity to receive electrons at the MS surface and augment inhibition efficiency [107,108].

To further analyze the molecular characteristics, each atom within the examined inhibitors was assigned a number, and their electrophilic and nucleophilic Fukui function indices are depicted in Fig. 16. The Fukui index outcomes unveil that both DAMD and HDMZ exhibit a significant quantity of active sites able to interact with the iron surface. This underscores the significance of electron donor and acceptor properties in the corrosive solution, amplifying their corrosion protection capabilities. Ultimately, these results validate the experimental findings, affirming that the molecules provide robust protection against mild steel corrosion under the acidic conditions of HCl 15 % [109].

To gain deeper insight into the intermolecular interactions within the complex structure, the DFT method was utilized to analyze the charge-transfer dynamics and the fundamental properties of the HDMZ complex. In this context, the electrostatic potential (ESP) represents a scalar field that characterizes the electrostatic forces within a molecular structure. Regions with positive ESP values signify areas of low electron density (indicating a positive charge), while negative ESP values point to areas of higher electron density (indicating a negative charge). ESP is commonly employed to investigate and anticipate various molecular attributes, such as reactivity and interactions between molecules. In Fig. 17a, the ESP analysis reveals that the N and O atoms in HDMZ display elevated electron density, suggesting their potential to interact with other groups to form the complex, as highlighted by the red coloring in the corresponding ESP region. Given that intermolecular interactions can impact the adsorption behavior of molecules on a metallic surface, we performed the reduced density gradient (RDG) analysis to identify both hydrogen bonds and weaker interaction regions in the HDMZ complex. By evaluating the RDG analysis, we can better understand the nature of these intermolecular forces and their influence on molecular adsorption. The RDG analysis for HDMZ was carried out, with the results displayed in Fig. 17b. The RDG isosurface and scatter plot illustrate the intensity and nature of noncovalent interactions via the sign(λ_2)ρ function, where different colors represent varying interaction strengths [95,96]. The structures exhibit van der Waals (vdW) interactions across multiple regions, indicating that the system has optimized into its most stable configuration, with vdW forces and hydrogen bonds with Zn through the involvement of OH groups. In line with the RDG visualization, the scatter plot in Fig. 17c displays a scattered region at lower RDG values, reinforcing that this anion exhibits vdW interactions and steric effects. Regions with varying RDG values correspond to different interaction strengths: high RDG values indicate strong covalent interactions, while lower values represent weak interactions or areas with no significant interactions. This effect is mainly influenced by bonding interactions within the complex. The key advantage of incorporating the complex is its ability to minimize steric hindrance, leading to stronger and more effective binding between HDMZ and the surface. This enhanced binding improves the overall efficiency and performance of the anticorrosion system.

3.9.2. First-principles DFTB calculations

DFT calculations offer a more precise and intricate depiction of the interactions occurring between the inhibitor and the iron surface [110]. These simulations not only reveal the most stable configurations and orientations for adsorption but also facilitate the computation of different properties like interaction energies, adsorption energies, and the projected density of states (PDOS). As a result, they enhance our understanding of the atomic-level interactions between the inhibitor and the MS surface. Fig. 18 illustrates the adsorption structure with the highest stability of DAMD and HDMZ on the Fe surface, determined through geometric optimization employing first-principles DFT simulations [111].

Observations reveal that the DAMD and HDMZ molecules adhere to the Fe surface in a flat orientation, underscoring the stability and consistency of their adsorption behavior. In the case of HDMZ, the molecule predominantly interacts through its oxygen, carbon and nitrogen atoms, establishing robust covalent bonds with the iron surface. On the other hand, DAMD adheres through carbon, leading to the formation of multiple bonds between the inhibitor and the iron surface. Evaluating the strength of inhibitor-iron surface interactions through computed adsorption energies, both DAMD and HDMZ exhibit negative values, suggesting exothermic processes and favorable adsorption on the Fe surface. Notably, HDMZ marginally higher adsorption energy (1.49 eV) in comparison to DAMD (1.05 eV). This implies that HDMZ possesses a more robust interaction with the MS surface, suggesting its potential as a corrosion inhibitor with higher efficacy.

Furthermore, a PDOS analysis provides the robust adsorption characteristics of DAMD and HDMZ on the Fe surface (Fig. 19), revealing significant overlap between the inhibitor's molecular orbitals and the Fe d-orbitals. This points to a substantial electronic interaction between the inhibitor molecules and the iron surface, reinforcing their stability and potential effectiveness in inhibiting corrosion. In summary, the outcomes of computational simulations, including analyses of adsorption behavior, bonding distances, adsorption energies, and electronic interactions, collectively indicate that both DAMD and HDMZ serve as effective inhibitors for mild steel in 15 % HCl corrosive media [112,113].

3.9.3. MD modeling

Examining the design of inhibitor molecules and their interactions with metal surfaces, such as Fe (110), is effectively facilitated through MD simulations. Fig. 20 illustrates the optimized adsorption geometries of HDMZ (Fig. 20a,b,c) and DAMD (Fig. 20a',b',c'), which exhibit stability in a parallel arrangement on the Fe (110) surface, as depicted in both top and side views. These molecules

Table 5
Calculated quantum chemical descriptors for DAMD and HDMZ molecules using DFT/GGA theoretical model. All quantum parameters are presented in eV.

Parameters Molecules	E_{HOMO}	E_{LUMO}	IP	EA	ΔE_{gap}	χ_{inh}	η_{inh}	ΔN_{inh}
DAMD	−5.457	−2.515	5.457	2.515	2.942	3.986	1.471	0.283
HDMZ	−5.194	−2.235	5.194	2.235	2.959	3.714	1.479	0.469

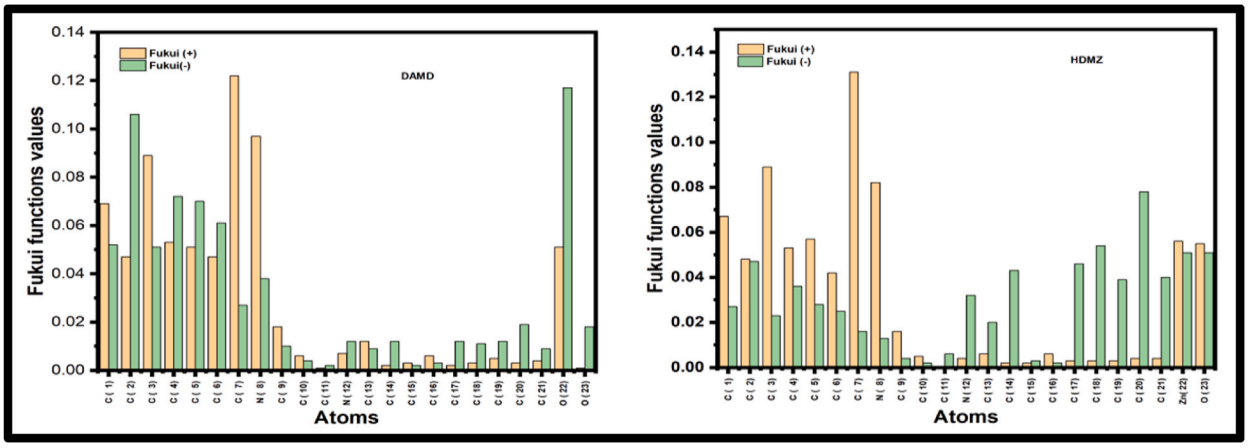

Fig. 16. Fukui indices values for nucleophilic and electrophilic attack for the same two inhibitor molecules HDMZ and DAMD. These values were also determined using the theoretical DFT/GGA model.

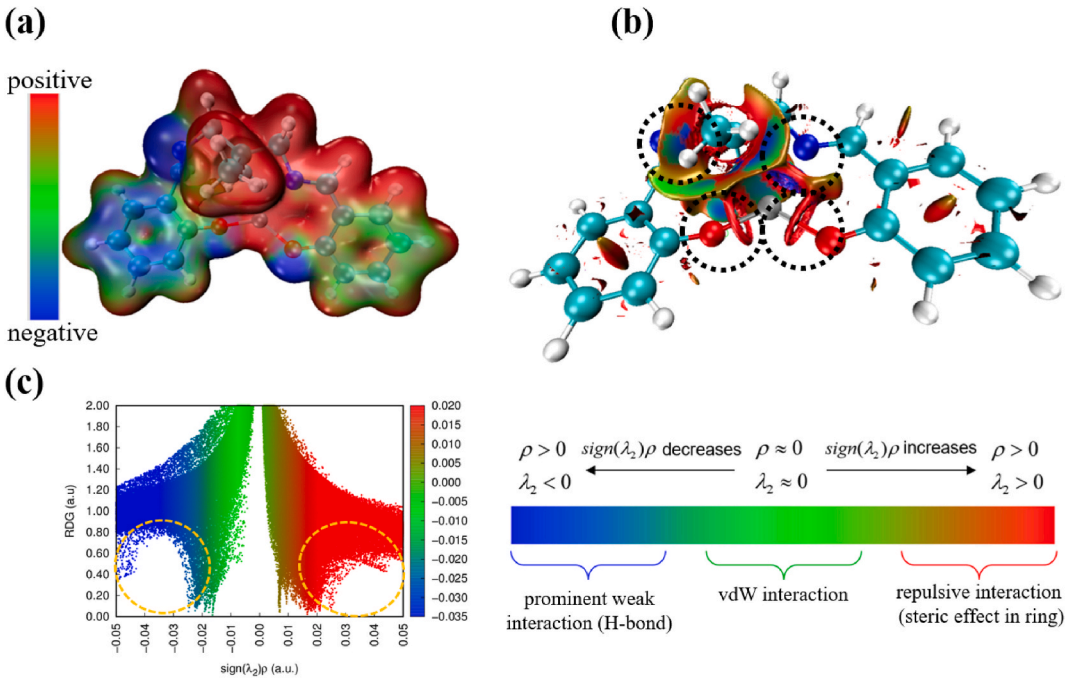

Fig. 17. (a) ESP distribution, (b) RDG visualization, and (c) RDG scattered plot of HDMZ complex.

feature focused heteroatoms (oxygen and nitrogen), polar functional groups, and π-bonds that promote robust interactions with the unoccupied 3d atomic orbitals of Fe (110) [114–116]. Upon optimizing the adsorption configuration, molecules of this kind are capable of providing comprehensive surface coverage, influencing the proximity of Fe atoms. Moreover, a deeper understanding of the role of solvent particles enhances our precision in comprehending how these molecules effectively function as corrosion inhibitors. In

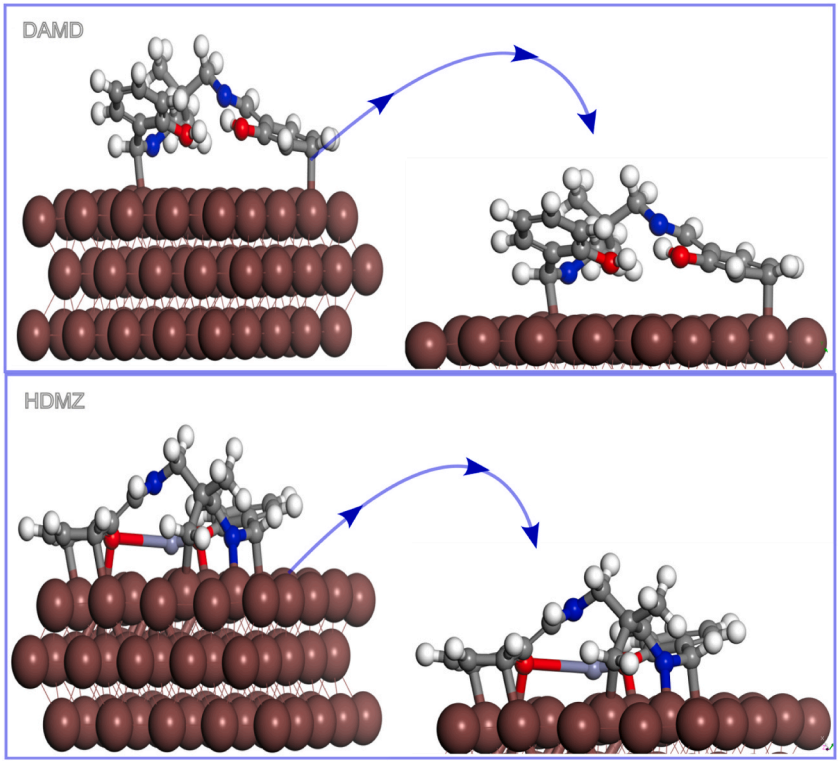

Fig. 18. First-principles DFT-optimized adsorption geometries of HDMZ and DAMD on the Fe (110) surface.

simpler terms, inhibitor molecules align parallel to the iron surface, facilitating penetration [117]. Consequently, a protective layer forms more uniformly over the metal surface, effectively hindering the ingress of detrimental substances, such as Cl^- ions, and thereby reducing corrosion [114,117].

3.10. Corrosion protection mechanism for mild steel in 15 % HCl solution

According to the experimental and computational findings presented, a proposed adsorption of corrosion inhibitors mechanism on MS in 15 % HCl solution is outlined in Fig. 21. Initially, the corrosion inhibitors undergo physisorption where they are electrostatically attracted to the negatively charged metal interface. This is followed by chemisorption, where covalent bonds are formed between the inhibitor molecules and the Fe atoms on the steel surface, resulting in formation of a protective layer [118,119]. The protective film formed during the chemisorption stage is believed to be the main factor contributing to the protection of mild steel corrosion in HCl solution [120]. This film acts as a barrier, preventing the corrosive ions from reaching the metal surface and thus reducing the rate of corrosion [121]. Besides the physisorption and chemisorption mechanisms, a comprehensive understanding of the molecular characteristics of the inhibitors, validates the experimental findings and affirms the robust protection provided by the molecules against mild steel corrosion in the acidic conditions of 15 % HCl [122]. In addition to the aforementioned mechanisms, the molecular dynamics simulations further support the proposed protective mechanism by illustrating the optimized adsorption geometries of the inhibitor molecules, exhibiting stability in a parallel arrangement on the Fe surface. This alignment facilitates the formation of a protective layer that effectively hinders the ingress of detrimental substances, thereby reducing corrosion [82]. The combined insights from the experimental, computational, and MD modeling studies present a deep understanding and validation of the proposed corrosion inhibition mechanism, shedding light on the efficacy of the inhibitors in mitigating mild steel corrosion in 15 % HCl solution.

4. Conclusion

This study provides a comprehensive evaluation of the synthesized Schiff base DAMD and its Zn complex HDMZ as corrosion inhibitors for mild steel in 15 % HCl solution. By employing a combination of experimental techniques—including weight loss measurements, EIS, PDP measurements, and SEM analysis, along with computational methods such as DFT, MD simulations, and SCC-DFTB calculations, significant insights were gained into the corrosion inhibition mechanisms of these compounds.

The key findings are summarized as follows.

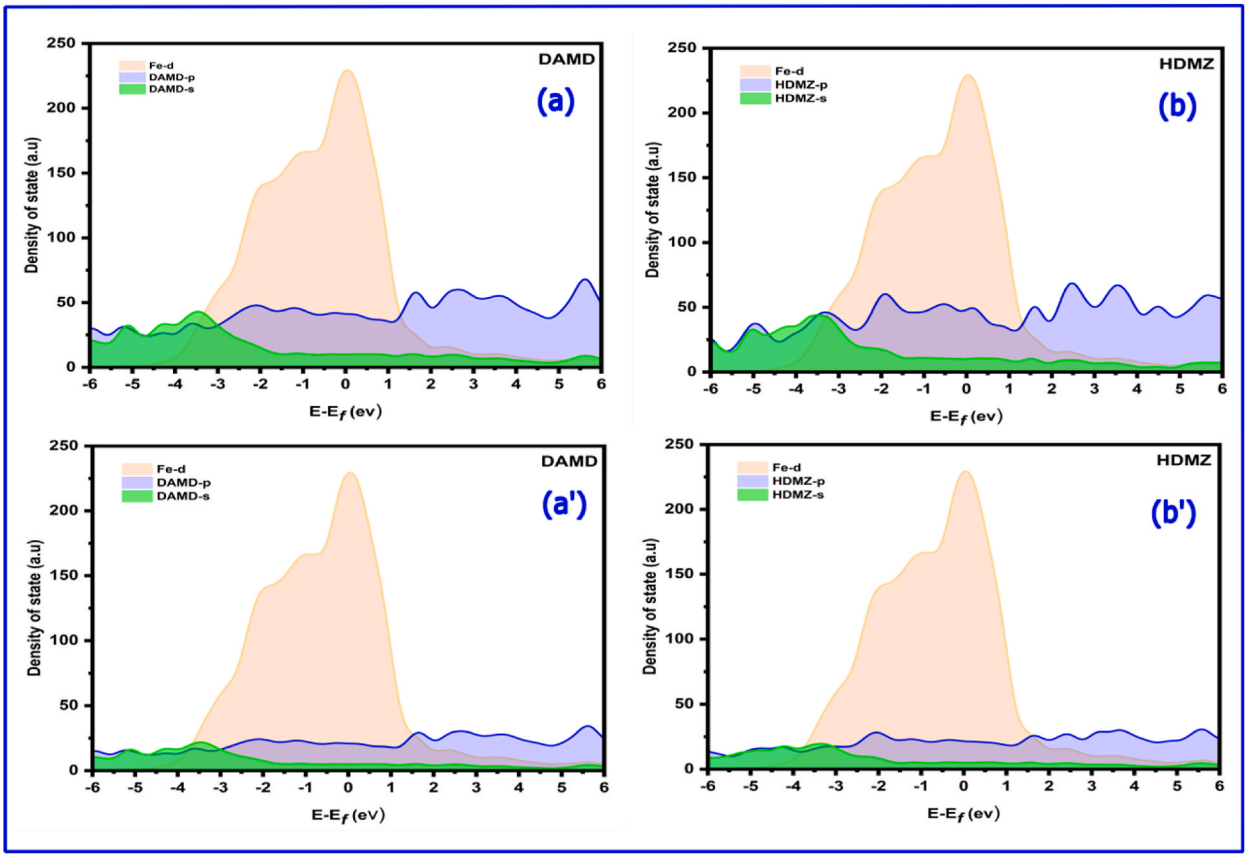

Fig. 19. Projected density of states (PDOS) for isolated and adsorbed DAMD and HDMZ molecules on the Fe (110) surface. (a, b) PDOS of isolated molecules positioned 7 Å above the highest iron layer and (b, b') PDOS of the adsorbed molecules. A Fermi energy point is chosen as a reference for the zero-energy state.

1. High inhibition efficiency: Both DAMD and HDMZ demonstrated excellent corrosion inhibition, with efficiencies of 90.44 % and 94.60 % respectively, at the maximum concentration (10^{-3} M). This highlights their strong potential for mitigating corrosion in aggressive environments. During immersion time tests HDMZ exhibited a continuous decrease in inhibition efficiency over time, indicating a gradual loss of inhibitory action.
2. Time-dependent efficacy: The study revealed that HDMZ experienced a gradual decline in inhibition efficiency during prolonged immersion, suggesting the need for further investigation into the long-term stability and durability of these inhibitors.
3. Adsorption mechanism: Adsorption of the inhibitors followed the Langmuir isotherm model, indicating strong monolayer coverage and significant interaction with the mild steel surface, which was further confirmed through SEM analysis.
4. Computational validation: Computational methods, including DFTB and MD simulations, provided crucial insights into the electronic structure and adsorption behavior of the inhibitors, affirming their stability and practical viability in industrial applications.

While this study demonstrates the effectiveness of DAMD and HDMZ as corrosion inhibitors, further research is required to address the limitations observed. In particular, future work should focus on a more detailed analysis of the inhibitors' long-term performance in varying industrial conditions, such as temperature fluctuations, pH variations, and the presence of other corrosive species. Additionally, exploring modifications to the chemical structure of these inhibitors may enhance their stability and adsorption characteristics, ensuring more consistent performance over extended periods. In summary, this study establishes DAMD and HDMZ as highly promising corrosion inhibitors for mild steel in 15 % HCl solution. Their high inhibition efficiency, strong adsorption properties, and the formation of a protective surface film point to significant industrial relevance.

CRediT authorship contribution statement

Badr El-Haitout: Writing – original draft, Data curation, Conceptualization. **Ratnaningsih Eko Sardjono:** Writing – original draft, Visualization. **Bouchra Es-Sounni:** Formal analysis, Data curation. **Maryam Chafiq:** Writing – review & editing, Writing – original draft, Methodology, Investigation. **Rachid Salghi:** Investigation, Formal analysis, Data curation. **Mohamed Bakhouch:** Formal analysis, Data curation. **Aisha H. Al-Moubaraki:** Funding acquisition, Formal analysis. **Jamilah M. Al-Ahmari:** Formal analysis, Data

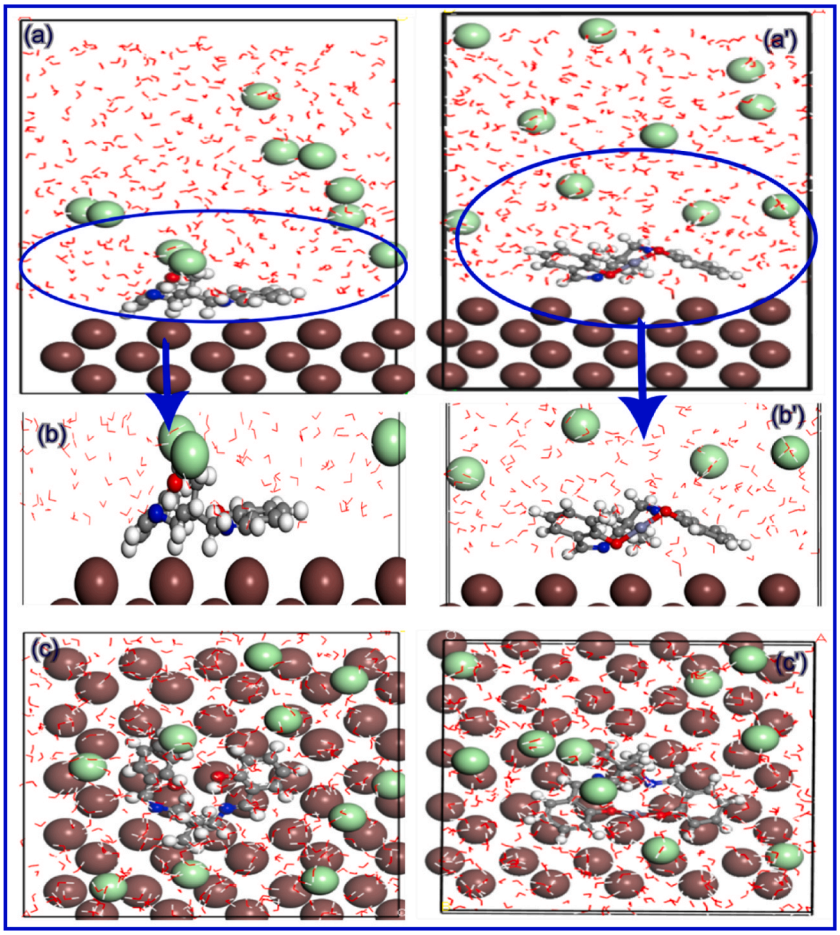

Fig. 20. Stable configuration of DAMD (a,b,c) and HDMZ (a',b',c') in an aqueous system. representations are provided, and molecular dynamics simulations determine these configurations.

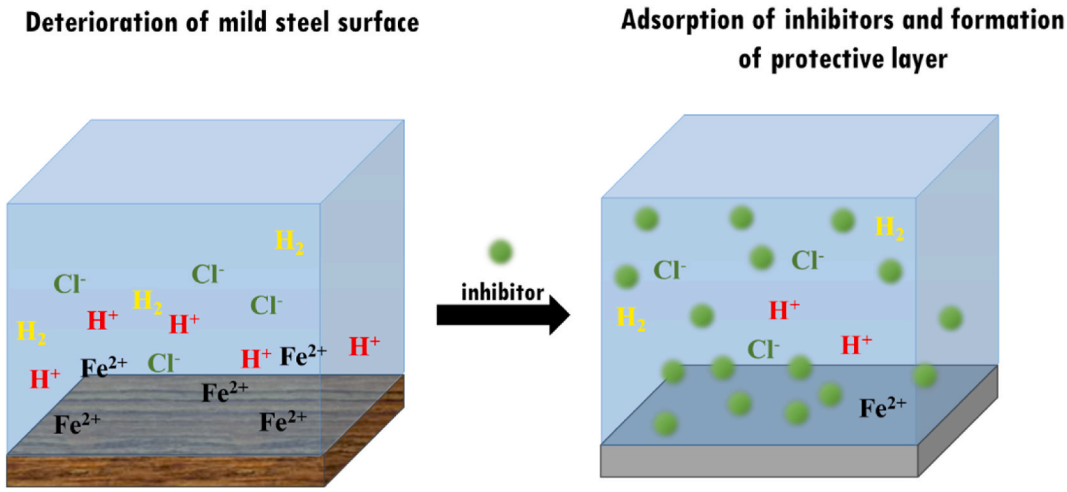

Fig. 21. A graphical representation of the corrosion inhibition mechanism representing different interactions between inhibitor molecules and mild steel surface.

curation. **Azza A. Al-Ghamdi:** Formal analysis, Data curation. **Mohammed Fahim:** Formal analysis, Data curation. **Belkheir Hammouti:** Data curation. **Abdelkarim Chaouiki:** Writing – review & editing, Writing – original draft, Validation, Investigation, Funding acquisition, Conceptualization. **Young Gun Ko:** Writing – review & editing.

Data availability

The data related to this work can be obtained from the corresponding authors upon reasonable request.

Declaration of competing interest

The authors declare that they have no known competing financial interests or personal relationships that could have appeared to influence the work reported in this paper.

References

[1] R.W. Revie, Corrosion and Corrosion Control: an Introduction to Corrosion Science and Engineering, John Wiley & Sons, 2008.
[2] T.K. Sarkar, V. Saraswat, R.K. Mitra, I.B. Obot, M. Yadav, Mitigation of corrosion in petroleum oil well/tubing steel using pyrimidines as efficient corrosion inhibitor: experimental and theoretical investigation, Mater. Today Commun. 26 (2021) 101862.
[3] V.S. Sastri, Types of Corrosion Inhibitor for Managing Corrosion in Underground Pipelines, Underground Pipeline Corrosion, 2014, pp. 166–211.
[4] G. Palanisamy, Corrosion inhibitors. Corrosion Inhibitors, 2019, pp. 1–24.
[5] N.R. Council, Research opportunities in corrosion science and engineering (2011).
[6] B. Tan, Y. Liu, Z. Gong, X. Zhang, J. Chen, L. Guo, J. Xiong, J. Liu, R. Marzouki, W. Li, Pyracantha fortuneana alcohol extracts as biodegradable corrosion inhibitors for copper in H2SO4 media, J. Mol. Liq. 397 (2024) 124117.
[7] R. Salim, E. Ech-chihbi, Y. Fernine, M. Koudad, L. Guo, E. Berdimurodov, M. Azam, Z. Rais, M. Taleb, Inhibition behavior of new ecological corrosion inhibitors for mild steel, copper and aluminum in acidic environment: theoretical and experimental investigation, J. Mol. Liq. 393 (2024) 123579.
[8] A. Fellah, Y. Harek, I. Ichchou, L. Larabi, H. Rouabhi, R. Bourzami, A. Ammari, Experimental and DFT studies of a novel salicylhydrazone derivative as a steel corrosion inhibitor, Colloids Surf. A Physicochem. Eng. Asp. 685 (2024) 133150.
[9] N. Tiwari, R.K. Mitra, M. Yadav, Corrosion protection of petroleum oil well/tubing steel using thiadiazolines as efficient corrosion inhibitor: experimental and theoretical investigation, Surface. Interfac. 22 (2021) 100770.
[10] V. Srivastava, M. Salman, D.S. Chauhan, S. Abdel-Azeim, M.A. Quraishi, (E)-2-styryl-1H-benzo [d] imidazole as novel green corrosion inhibitor for carbon steel: experimental and computational approach, J. Mol. Liq. 324 (2021) 115010.
[11] B.E. Brycki, I.H. Kowalczyk, A. Szulc, O. Kaczerewska, M. Pakiet, Organic corrosion inhibitors, corrosion inhibitors, Principles and Recent Applications 3 (2018) 33.
[12] I. Pradipta, D. Kong, J.B.L. Tan, Natural organic antioxidants from green tea form a protective layer to inhibit corrosion of steel reinforcing bars embedded in mortar, Construct. Build. Mater. 221 (2019) 351–362.
[13] B. Tan, Y. Liu, H. Ren, Z. Gong, X. Li, W. Li, L. Guo, R. Chen, J. Wei, Q. Dai, N, S-carbon quantum dots as inhibitor in pickling process of heat exchangers for enhanced performance in multi-stage flash seawater desalination, Desalination 589 (2024) 117969.
[14] H. Ren, Y. Liu, Z. Gong, B. Tan, H. Deng, J. Xiong, P. Shao, Q. Dai, J. Cao, R. Marzouki, Pumpkin leaf extract crop waste as a new degradable and environmentally friendly corrosion inhibitor, Langmuir 40 (2024) 5738–5752, https://doi.org/10.1021/acs.langmuir.3c03399.
[15] S.L. Li, Y.G. Wang, S.H. Chen, R. Yu, S.B. Lei, H.Y. Ma, D.X. Liu, Some aspects of quantum chemical calculations for the study of Schiff base corrosion inhibitors on copper in NaCl solutions, Corrosion Sci. 41 (1999) 1769–1782, https://doi.org/10.1016/S0010-938X(99)00014-1.
[16] C. Verma, M.A. Quraishi, Recent progresses in Schiff bases as aqueous phase corrosion inhibitors: design and applications, Coord. Chem. Rev. 446 (2021) 214105, https://doi.org/10.1016/j.ccr.2021.214105.
[17] K.C. Gupta, A.K. Sutar, Catalytic activities of Schiff base transition metal complexes, Coord. Chem. Rev. 252 (2008) 1420–1450, https://doi.org/10.1016/j.ccr.2007.09.005.
[18] H.F. Abd El-halim, M.M. Omar, G.G. Mohamed, Synthesis, structural, thermal studies and biological activity of a tridentate Schiff base ligand and their transition metal complexes, Spectrochim. Acta Mol. Biomol. Spectrosc. 78 (2011) 36–44, https://doi.org/10.1016/j.saa.2010.06.003.
[19] T. Benali, A. Bouyahya, K. Habbadi, G. Zengin, A. Khabbach, E.H. Achbani, K. Hammani, Chemical composition and antibacterial activity of the essential oil and extracts of Cistus ladaniferus subsp. ladanifer and Mentha suaveolens against phytopathogenic bacteria and their ecofriendly management of phytopathogenic bacteria, Biocatal. Agric. Biotechnol. 28 (2020) 101696, https://doi.org/10.1016/j.bcab.2020.101696.
[20] Department of Chemistry, College of Science, Al-Nahrain University, Iraq Baghdad, F.M. Ibrahim, S.M. Abdalhadi, Department of Remote Sensing, College of Remote Sensing and Geophysics, Al-Karkh University of Science, Baghdad, Iraq, performance of schiff bases metal complexes and their ligand in biological activity: a review, ANJS 24 (2021) 1–10, https://doi.org/10.22401/ANJS.24.1.01.
[21] A.A. Azez, R.T. Natheer, E.R. Mohammed, M.Y. Saleh, Preparation of new complexes of Fe(II), Co(II), Ni(II) and Cu(II) with mixed ligands of ciprofloxacin or levofloxacin with eugenol and study of their chemical and physical properties, Egypt. J. Chem. 64 (2021) 3991–3996, https://doi.org/10.21608/ejchem.2021.63144.3352.
[22] B. Es-Sounni, E.M. Haily, A. Nakkabi, M. Bakhouch, L. Bejaoui, S. Kaya, M. El Yazidi, L. Bih, M. Saadi, L. El Ammari, New Bi-nuclear nickel (II) complex-based salen schiff base: synthesis, crystal structure, spectroscopic, thermal, and electrical investigations, Chemistry 4 (2022) 1193–1207.
[23] B. Es-Sounni, A. Nakkabi, A. Bouymajane, I. Elaaraj, M. Bakhouch, F.R. Filali, M. El Yazidi, N. El Moualij, M. Fahim, Synthesis, characterization, antioxidant and antibacterial activities of six metal complexes based tetradentate salen type bis-Schiff base, Biointerface Res. Appl. Chem 13 (2023) 333.
[24] A. Berhanu, G. No, I. Mohiuddin, A. Malik, J.S. Aulakh, V. Kumar, K.-H. Kim, A review of the applications of Schiff bases as optical chemical sensors, TrAC, Trends Anal. Chem. 116 (2019) 74–91, https://doi.org/10.1016/j.trac.2019.04.025.
[25] H. Ahchouch, A. Chaouiki, A.H. Al-Moubaraki, J.M. Al-Ahmari, A.A. Al-Ghamdi, L. Bammou, M. Belkhaouda, M. Chafiq, Y.G. Ko, Fabrication of protective organic layer using schiff-base metal complex responsible for excellent corrosion performance: experimental and theoretical perspectives, ACS Omega 9 (2024) 15015–15029, https://doi.org/10.1021/acsomega.3c09097.
[26] C. Boulechfar, H. Ferkous, A. Delimi, M. Berredjem, A. Kahlouche, A. Madaci, S. Djellali, S. Boufas, A. Djedouani, A. Errachid, Corrosion inhibition of Schiff base and their metal complexes with [Mn (II), Co (II) and Zn (II)]: experimental and quantum chemical studies, J. Mol. Liq. 378 (2023) 121637.
[27] S. Kashyap, S. Kumar, K. Ramasamy, S.M. Lim, S.A.A. Shah, H. Om, B. Narasimhan, Synthesis, biological evaluation and corrosion inhibition studies of transition metal complexes of Schiff base, Chem. Cent. J. 12 (2018) 117, https://doi.org/10.1186/s13065-018-0487-1.
[28] H.M. Abd El-Lateef, K.A. Soliman, M.A. Al-Omair, M.S.S. Adam, A combination of modeling and experimental approaches to investigate the novel nicotinohydrazone Schiff base and its complexes with Zn (II) and ZrO (II) as inhibitors for mild-steel corrosion in molar HCl, J. Taiwan Inst. Chem. Eng. 120 (2021) 391–408.
[29] M. Mishra, K. Tiwari, P. Mourya, M.M. Singh, V.P. Singh, Synthesis, characterization and corrosion inhibition property of nickel (II) and copper (II) complexes with some acylhydrazine Schiff bases, Polyhedron 89 (2015) 29–38.

[30] A.S. Fouda, M.A. Ismail, M.A. Khaled, A.A. El-Hossiany, Experimental and computational chemical studies on the corrosion inhibition of new pyrimidinone derivatives for copper in nitric acid, Sci. Rep. 12 (2022) 16089, https://doi.org/10.1038/s41598-022-20306-4.

[31] A.A. Al-Amiery, A.B. Mohamad, A.A.H. Kadhum, L.M. Shaker, W.N.R.W. Isahak, M.S. Takriff, Experimental and theoretical study on the corrosion inhibition of mild steel by nonanedioic acid derivative in hydrochloric acid solution, Sci. Rep. 12 (2022) 4705, https://doi.org/10.1038/s41598-022-08146-8.

[32] H. Namdar-Asl, F. Fakheri, S. Pour-Ali, R. Tavangar, S. Hejazi, Synthesis and corrosion inhibition study of 1-aminobenzotriazole for mild steel in HCl solution: electrochemical, surface analysis, and theoretical investigations, Progress in Color, Colorants and Coatings 17 (2024) 61–74.

[33] S. Wan, R.C. Sinclair, P.V. Coveney, Uncertainty quantification in classical molecular dynamics, Phil. Trans. R. Soc. A. 379 (82) (2021) 20200082, https://doi.org/10.1098/rsta.2020.0082 rsta.2020.

[34] B. El-Haitout, I. Selatnia, H. Lgaz, M.R. Al-Hadeethi, H.-S. Lee, A. Chaouiki, Y.G. Ko, I.H. Ali, R. Salghi, Exploring the feasibility of new eco-friendly heterocyclic compounds for establishing efficient corrosion protection for N80 steel in a simulated oil well acidizing environment: from molecular-level prediction to experimental validation, Colloids Surf. A Physicochem. Eng. Asp. 656 (2023) 130372.

[35] B. El-Haitout, H. Lgaz, M.R. Al-Hadeethi, H.-S. Lee, R.J. Adnin, M. Messali, K. Haboubi, L. Bazzi, R. Salghi, Surface interaction and inhibition mechanisms of hydrazide derivatives on N80 steel in acidizing media: a comprehensive analysis through experimental and theoretical methods, Chem. Phys. Lett. (2023) 140980.

[36] A. Al-Amiery, T.A. Salman, K.F. Alazawi, L.M. Shaker, A.A.H. Kadhum, M.S. Takriff, Quantum chemical elucidation on corrosion inhibition efficiency of Schiff base: DFT investigations supported by weight loss and SEM techniques, Int. J. Low Carbon Technol. 15 (2020) 202–209, https://doi.org/10.1093/ijlct/ctz074.

[37] S. Bashir, A. Thakur, H. Lgaz, I.-M. Chung, A. Kumar, Corrosion inhibition efficiency of bronopol on aluminium in 0.5 M HCl solution: insights from experimental and quantum chemical studies, Surface. Interfac. 20 (2020) 100542, https://doi.org/10.1016/j.surfin.2020.100542.

[38] D.N. Avram, C.M. Davidescu, M.L. Dan, J.C. Mirza-Rosca, I. Hulka, A. Pascu, E.M. Stanciu, Electrochemical evaluation of protective coatings with Ti additions on mild steel substrate with potential application for PEM fuel cells, Materials 15 (2022) 5364, https://doi.org/10.3390/ma15155364.

[39] A. Saxena, D. Prasad, K.K. Thakur, J. Kaur, PDP, EIS, and surface studies of the low-carbon steel by the extract of tinospora cordifolia: a green approach to the corrosion inhibition, Arabian J. Sci. Eng. 46 (2021) 425–436, https://doi.org/10.1007/s13369-020-04894-9.

[40] Y. Lei, Z. Qiu, N. Tan, H. Du, D. Li, J. Liu, T. Liu, W. Zhang, X. Chang, Polyaniline/CeO2 nanocomposites as corrosion inhibitors for improving the corrosive performance of epoxy coating on carbon steel in 3.5% NaCl solution, Prog. Org. Coating 139 (2020) 105430, https://doi.org/10.1016/j.porgcoat.2019.105430.

[41] Study of Corrosion Behavior of N'-, (2-(2-oxomethylpyrrol-1-yl)ethyl)piperidine for mild steel in the acid environment, Biointerface Res Appl Chem 12 (2021) 3638–3646, https://doi.org/10.33263/BRIAC123.36383646.

[42] H. Ahchouch, A. Chaouiki, A.H. Al-Moubaraki, J.M. Al-Ahmari, A.A. Al-Ghamdi, L. Bammou, M. Belkhaouda, M. Chafiq, Y.G. Ko, Fabrication of protective organic layer using schiff-base metal complex responsible for excellent corrosion performance: experimental and theoretical perspectives, ACS Omega 9 (2024) 15015–15029, https://doi.org/10.1021/acsomega.3c09097.

[43] O. Amrhar, H.-S. Lee, H. Lgaz, A. Berisha, E.E. Ebenso, Y. Cho, Computational insights into the adsorption mechanisms of anionic dyes on the rutile TiO2 (1 1 0) surface: combining SCC-DFT tight binding with quantum chemical and molecular dynamics simulations, J. Mol. Liq. 377 (2023) 121554, https://doi.org/10.1016/j.molliq.2023.121554.

[44] N.B. Iroha, N.A. Madueke, V. Mkpenie, B.T. Ogunyemi, L.A. Nnanna, S. Singh, E.D. Akpan, E.E. Ebenso, Experimental, adsorption, quantum chemical and molecular dynamics simulation studies on the corrosion inhibition performance of Vincamine on J55 steel in acidic medium, J. Mol. Struct. 1227 (2021) 129533, https://doi.org/10.1016/j.molstruc.2020.129533.

[45] S. Chang, Q. Zhang, Y. Lu, S. Wu, W. Wang, High-efficiency and selective adsorption of organic pollutants by magnetic CoFe2O4/graphene oxide adsorbents: experimental and molecular dynamics simulation study, Separ. Purif. Technol. 238 (2020) 116400, https://doi.org/10.1016/j.seppur.2019.116400.

[46] A. Chaouiki, M. Chafiq, Y.G. Ko, Nature-inspired architecture combining organic–inorganic frameworks: unique structure and active sites toward a stable anti-corrosion coating, Appl. Mater. Today 32 (2023) 101852.

[47] A. Batah, A.H. Al-Moubaraki, E.A. Noor, J.M. Al-Ahmari, A.A. Al-Ghamdi, O. Id El Mouden, R. Salghi, M. Chafiq, A. Chaouiki, Y.G. Ko, Environmentally benign grape seed oil for corrosion inhibition: cutting-edge computational modeling techniques revealing the intermolecular and intramolecular synergistic inhibition action, Coatings 14 (2024) 77.

[48] A.H. Al-Moubaraki, A. Chaouiki, J.M. Alahmari, W.A. Al-Hammadi, E.A. Noor, A.A. Al-Ghamdi, Y.G. Ko, Development of natural plant extracts as sustainable inhibitors for efficient protection of mild steel: experimental and first-principles multi-level computational methods, Materials 15 (2022) 8688.

[49] O. Id El Mouden, A.H. Al-Moubaraki, M. Chafiq, M. Bakhouch, A. Batah, L. Bammou, M. Belkhaouda, A. Chaouiki, Y.G. Ko, BMPD-assisted enhancement of corrosion resistance of carbon steel: experimental and first-principle DFTB insights, Metals 14 (2024) 69.

[50] S. Peng, J. Xu, D. Hu, Z.-H. Xie, P. Munroe, The impact of surface scratches on the corrosion behavior of nanocrystalline high entropy alloy coatings: electrochemical experiments and first-principles study, Appl. Mater. Today 31 (2023) 101767, https://doi.org/10.1016/j.apmt.2023.101767.

[51] M. Boudalia, R.M. Fernández-Domene, L. Guo, S. Echihi, M.E. Belghiti, A. Zarrouk, A. Bellaouchou, A. Guenbour, J. García-Antón, Experimental and theoretical tests on the corrosion protection of mild steel in hydrochloric acid environment by the use of pyrazole derivative, Materials 16 (2023) 678.

[52] S. Wan, H. Chen, T. Zhang, B. Liao, X. Guo, Anti-corrosion mechanism of parsley extract and synergistic iodide as novel corrosion inhibitors for carbon steel-Q235 in acidic medium by electrochemical, XPS and DFT methods, Front. Bioeng. Biotechnol. 9 (2021) 815953.

[53] A. Bayaguud, Y. Fu, C. Zhu, Interfacial parasitic reactions of zinc anodes in zinc ion batteries: underestimated corrosion and hydrogen evolution reactions and their suppression strategies, J. Energy Chem. 64 (2022) 246–262.

[54] Q. Lu, L. Wang, J. Xin, H. Tian, X. Wang, Z. Cui, Corrosion evolution and stress corrosion cracking of E690 steel for marine construction in artificial seawater under potentiostatic anodic polarization, Construct. Build. Mater. 238 (2020) 117763.

[55] B. Heider, E. Scharifi, T. Engler, M. Oechsner, K. Steinhoff, Influence of heated forming tools on corrosion behavior of high strength aluminum alloys, Mater. Werkst. 52 (2021) 145–151, https://doi.org/10.1002/mawe.202000125.

[56] F.H. Zaidon, K. Kassim, H.M. Zaki, Z. Embong, N.Z.N. Hashim, Adsorption and corrosion inhibition accomplishment for thiosemicarbazone derivatives for mild steel in 1.0 M HCl medium: electrochemical, XPS and DFT studies, J. Mol. Liq. 329 (2021) 115553.

[57] N.Z.N. Hashim, M.A.M. Kahar, K. Kassim, Z. Embong, Experimental and theoretical studies of azomethines derived from benzylamine as corrosion inhibitors of mild steel in 1 M HCl, J. Mol. Struct. 1222 (2020) 128899.

[58] H. Ahchouch, A. Chaouiki, S.A. Talhajt, L. Bammou, M. Belkhaouda, R. Salghi, Y.G. Ko, Inter-and intra-molecular synergism in designing MgO-MCC composite-based coating: an efficient inhibitor for excellent anticorrosion performance, Process Saf. Environ. Protect. 177 (2023) 1461–1476.

[59] M. Chafiq, A. Chaouiki, H. Lgaz, K.V. Bhaskar, K.S. Bhat, I.H. Ali, Electrochemical and theoretical analysis of a novel spirocyclopropane derivative for corrosion inhibition of mild steel in acidic medium, Applied Journal of Environmental Engineering Science 6 (2020).

[60] E. Ech-chihbi, M. Adardour, W. Ettahiri, R. Salim, M. Ouakki, M. Galai, A. Baouid, M. Taleb, Surface interactions and improved corrosion resistance of mild steel by addition of new triazolyl-benzimidazolone derivatives in acidic environment, J. Mol. Liq. 387 (2023) 122652.

[61] K. Azzaoui, E. Mejdoubi, S. Jodeh, A. Lamhamdi, E. Rodriguez-Castellón, M. Algarra, A. Zarrouk, A. Errich, R. Salghi, H. Lgaz, Eco friendly green inhibitor Gum Arabic (GA) for the corrosion control of mild steel in hydrochloric acid medium, Corrosion Sci. 129 (2017) 70–81.

[62] A. Chaouiki, M. Chafiq, M. Rbaa, H. Lgaz, R. Salghi, B. Lakhrissi, I.H. Ali, S. Masroor, Y. Cho, New 8-hydroxyquinoline-bearing quinoxaline derivatives as effective corrosion inhibitors for mild steel in HCl: electrochemical and computational investigations, Coatings 10 (2020) 811.

[63] M. Chafiq, A. Chaouiki, M. Damej, H. Lgaz, R. Salghi, I.H. Ali, M. Benmessaoud, S. Masroor, I.-M. Chung, Bolaamphiphile-class surfactants as corrosion inhibitor model compounds against acid corrosion of mild steel, J. Mol. Liq. 309 (2020) 113070.

[64] B. Tan, Z. Gong, W. He, J. Xiong, L. Guo, R. Marzouki, Insight into the anti-corrosion mechanism of crop waste Arachis hypogaea L. leaf extract for copper in sulfuric acid medium, Sustainable Chemistry and Pharmacy 38 (2024) 101449.

[65] M.E. Mashuga, L.O. Olasunkanmi, C. Verma, E.-S.M. Sherif, E.E. Ebenso, Experimental and computational mediated illustration of effect of different substituents on adsorption tendency of phthalazinone derivatives on mild steel surface in acidic medium, J. Mol. Liq. 305 (2020) 112844.

[66] F.D. Zhang, H. Liu, C. Suebka, Y.X. Liu, Z. Liu, W. Guo, Y.M. Cheng, S.L. Zhang, L. Li, Corrosion behaviour of laser-cleaned AA7024 aluminium alloy, Appl. Surf. Sci. 435 (2018) 452–461.

[67] Q. Tayyaba, M. Shahzad, A.Q. Butt, M. Khan, A.H. Qureshi, The influence of electrophoretic deposition of HA on Mg-Zn-Zr alloy on its in-vitro degradation behaviour in the Ringer's solution, Surf. Coating. Technol. 375 (2019) 197–204.

[68] L. Bousselmi, C. Fiaud, B. Tribollet, E. Triki, Impedance spectroscopic study of a steel electrode in condition of scaling and corrosion: interphase model, Electrochim. Acta 44 (1999) 4357–4363.

[69] K. Xhanari, Y. Wang, Z. Yang, M. Finšgar, A review of recent advances in the inhibition of sweet corrosion, Chem. Rec. 21 (2021) 1845–1875, https://doi.org/10.1002/tcr.202100072.

[70] W.L. Ma, H.X. Wang, R. Barker, N. Kapur, Y. Hua, A. Neville, Corrosion behaviour of X65 carbon steel under the intermittent oil/water wetting: a synergic effect of flow velocity and alternate immersion period, Corrosion Sci. 187 (2021) 109507.

[71] P. Bommersbach, C. Alemany-Dumont, J.-P. Millet, B. Normand, Formation and behaviour study of an environment-friendly corrosion inhibitor by electrochemical methods, Electrochim. Acta 51 (2005) 1076–1084.

[72] A.H. Al-Moubaraki, A. Al-Judaibi, M. Asiri, Corrosion of C-steel in the Red Sea: effect of immersion time and inhibitor concentration, Int. J. Electrochem. Sci. 10 (2015) 4252–4278.

[73] H. Jafari, K. Akbarzade, I. Danaee, Corrosion inhibition of carbon steel immersed in a 1 M HCl solution using benzothiazole derivatives, Arab. J. Chem. 12 (2019) 1387–1394.

[74] A.A. Alamiery, W. Isahak, H.S.S. Aljibori, H.A. Al-Asadi, A.A.H. Kadhum, Effect of the structure, immersion time and temperature on the corrosion inhibition of 4-pyrrol-1-yl-N-(2, 5-dimethyl-pyrrol-1-yl) benzoylamine in 1.0 M HCl solution, International Journal of Corrosion and Scale Inhibition 10 (2021) 700–713.

[75] C. Li, J. Wu, D. Zhang, P. Wang, Z. Sun, L. Zhu, Y. Gao, Y. Wan, Z. Yang, Y. Wang, Alternate immersion improves corrosion inhibition efficiency of Halomonas titanicae towards EH40 steel, Corrosion Sci. 206 (2022) 110503.

[76] M. Mobin, M. Parveen, R. Aslam, Effect of different additives, temperature, and immersion time on the inhibition behavior of L-valine for mild steel corrosion in 5% HCl solution, J. Phys. Chem. Solid. 161 (2022) 110422.

[77] D. Wang, Y. Li, B. Chen, L. Zhang, Novel surfactants as green corrosion inhibitors for mild steel in 15% HCl: experimental and theoretical studies, Chem. Eng. J. 402 (2020) 126219.

[78] R. Hsissou, B. Benzidia, M. Rehioui, M. Berradi, A. Berisha, M. Assouag, N. Hajjaji, A. Elharfi, Anticorrosive property of hexafunctional epoxy polymer HGTMDAE for E24 carbon steel corrosion in 1.0 M HCl: gravimetric, electrochemical, surface morphology and molecular dynamic simulations, Polym. Bull. 77 (2020) 3577–3601, https://doi.org/10.1007/s00289-019-02934-5.

[79] A.A. Alamiery, Study of corrosion behavior of N'-(2-(2-oxomethylpyrrol-1-yl) ethyl) piperidine for mild steel in the acid environment, Biointerface Res, Appl. Chem. 12 (2022) 3638–3646.

[80] A.A. Mansour, C. Hejjaj, F.Z. Thari, K. Karrouchi, L. Bazzi, K. Bougrin, H. Lgaz, M. Messali, H. Lee, R. Salghi, Interfacial phenomena and surface protection of N80-carbon steel in acidic environments using thiazolidinediones: an experimental and computational analysis, Colloids Surf. A Physicochem. Eng. Asp. 677 (2023) 132415.

[81] J. Wysocka, M. Cieslik, S. Krakowiak, J. Ryl, Carboxylic acids as efficient corrosion inhibitors of aluminium alloys in alkaline media, Electrochim. Acta 289 (2018) 175–192.

[82] A.K. Singh, S.K. Shukla, M.A. Quraishi, E.E. Ebenso, Investigation of adsorption characteristics of N, N′-[(methylimino) dimethylidyne] di-2, 4-xylidine as corrosion inhibitor at mild steel/sulphuric acid interface, J. Taiwan Inst. Chem. Eng. 43 (2012) 463–472.

[83] M. Lebrini, M. Traisnel, M. Lagrenée, B. Mernari, F. Bentiss, Inhibitive properties, adsorption and a theoretical study of 3, 5-bis (n-pyridyl)-4-amino-1, 2, 4-triazoles as corrosion inhibitors for mild steel in perchloric acid, Corrosion Sci. 50 (2008) 473–479.

[84] A.A. Khadom, A.S. Yaro, A.A.H. Kadhum, Adsorption mechanism of benzotriazole for corrosion inhibition of copper-nickel alloy in hydrochloric acid, J. Chil. Chem. Soc. 55 (2010) 150–152.

[85] R.L. Minagalavar, S.K. Rajappa, M.R. Rathod, A.M. Sajjan, Investigation of corrosion inhibition performance of expired fluconazole drug on mild steel in 0.5M H2SO4 medium, J. Mol. Liq. 391 (2023) 123291, https://doi.org/10.1016/j.molliq.2023.123291.

[86] Y. Boughoues, M. Benamira, L. Messaadia, N. Ribouh, Adsorption and corrosion inhibition performance of some environmental friendly organic inhibitors for mild steel in HCl solution via experimental and theoretical study, Colloids Surf. A Physicochem. Eng. Asp. 593 (2020) 124610, https://doi.org/10.1016/j.colsurfa.2020.124610.

[87] D. Patel, K. Makwana, M.B. Shirdhonkar, K.C. Kuperkar, A new insight into non-steroidal anti-inflammatory drugs (NSAIDs) as modulated green inhibitory agent on mild steel corrosion, ChemistrySelect 4 (2019) 5799–5809, https://doi.org/10.1002/slct.201900037.

[88] A. Chaouiki, M. Chafiq, H. Lgaz, M.R. Al-Hadeethi, I.H. Ali, S. Masroor, I.-M. Chung, Green corrosion inhibition of mild steel by hydrazone derivatives in 1.0 M HCl, Coatings 10 (2020) 640, https://doi.org/10.3390/coatings10070640.

[89] D. Kumar, V.M. K, V. Jain, B. Rai, Integrating experiments, DFT and characterization for comprehensive corrosion inhibition studies – a case for cinnamaldehyde as an excellent green inhibitor for steels in acidic media, Corrosion Sci. 208 (2022) 110623, https://doi.org/10.1016/j.corsci.2022.110623.

[90] Y. Wang, Y. Qiang, H. Zhi, B. Ran, D. Zhang, Evaluating the synergistic effect of maple leaves extract and iodide ions on corrosion inhibition of Q235 steel in H2SO4 solution, J. Ind. Eng. Chem. 117 (2023) 422–433, https://doi.org/10.1016/j.jiec.2022.10.030.

[91] G. Chen, J. Lin, Q. Liu, J. Zhang, Y. Wu, H. Li, C. Qu, W. Song, Corrosion inhibition and the structure-efficiency relationship study of two cationic surfactants, ACMM 66 (2019) 388–393, https://doi.org/10.1108/ACMM-10-2017-1856.

[92] K. Raviprabha, R.S. Bhat, Corrosion inhibition of mild steel in 0.5 M HCL by substituted 1,3,4-oxadiazole, Egyptian Journal of Petroleum 32 (2023) 1–10, https://doi.org/10.1016/j.ejpe.2023.03.002.

[93] M. Chafiq, A.H. Al-Moubaraki, A. Chaouiki, Y.G. Ko, A novel coating system based on layered double hydroxide/HQS hierarchical structure for reliable protection of Mg alloy: electrochemical and computational perspectives, Materials 17 (2024) 1176.

[94] A. Chaouiki, M. Chafiq, T. Suhartono, Y.G. Ko, Unveiling the in-situ formation mechanism of nano-fir tree-like architecture: yolk-shell structure enables the development of an advanced multifunctional template, Chem. Eng. J. (2023) 144355.

[95] M. Chafiq, A. Chaouiki, R. Salghi, Y.G. Ko, Fabrication of branch-like Aph@ LDH-MgO material through organic-inorganic hybrid conjugation for excellent anti-corrosion performance, J. Magnesium Alloys 11 (2023) 2469–2485.

[96] F. Hazmatulhaq, Y. Sheng, T. Suhartono, S. Fatimah, M. Chafiq, A. Chaouiki, Y.G. Ko, Electrochemical response and adsorption behavior of sulfocarbanilide inhibitor on oxide layer produced by pulsed plasma electrolysis (PPE): experimental and DFT perspective, Corrosion Sci. (2024) 111849.

[97] H. Gasparetto, Y. Vieira, N.P.G. Salau, The role of quantum-chemical descriptors and sigma-profile overlapping of different co-solvents on tuning ethanolic extraction of soybean oil, J. Mol. Liq. 384 (2023) 122306.

[98] H. Malik, H.W. Khan, M.U.H. Shah, M.I. Ahmad, I. Khan, A.A. Al-Kahtani, M. Sillanpää, Screening of ionic liquids as green entrainers for ethanol water separation by extractive distillation: COSMO-RS prediction and aspen plus simulation, Chemosphere 311 (2023) 136901.

[99] V. Srivastava, M. Salman, D.S. Chauhan, S. Abdel-Azeim, M.A. Quraishi, (E)-2-styryl-1H-benzo[d]imidazole as novel green corrosion inhibitor for carbon steel: experimental and computational approach, J. Mol. Liq. 324 (2021) 115010, https://doi.org/10.1016/j.molliq.2020.115010.

[100] R.K. Mehta, S.K. Gupta, M. Yadav, Studies on pyrimidine derivative as green corrosion inhibitor in acidic environment: electrochemical and computational approach, J. Environ. Chem. Eng. 10 (2022) 108499, https://doi.org/10.1016/j.jece.2022.108499.

[101] A. Dehghani, G. Bahlakeh, B. Ramezanzadeh, M. Ramezanzadeh, Potential role of a novel green eco-friendly inhibitor in corrosion inhibition of mild steel in HCl solution: detailed macro/micro-scale experimental and computational explorations, Construct. Build. Mater. 245 (2020) 118464, https://doi.org/10.1016/j.conbuildmat.2020.118464.

[102] A. Chaouiki, M. Chafiq, Y.G. Ko, Unveiling the mechanisms behind high CO_2 adsorption by the selection of suitable ionic liquids incorporated into a ZIF-8 metal organic framework: a computational approach, Environ. Res. 246 (2024) 118112.

[103] M. Chafiq, A. Chaouiki, T. Suhartono, F. Hazmatulhaq, Y.G. Ko, Interface engineering of LDH-based material as efficient anti-corrosive system via synergetic performance of host, interlayers, and morphological features of nature-mimic architectures, Chem. Eng. J. (2023) 142239.
[104] A.A. Alamiery, W.N.R. Wan Isahak, M.S. Takriff, Inhibition of mild steel corrosion by 4-benzyl-1-(4-oxo-4-phenylbutanoyl)thiosemicarbazide: gravimetrical, adsorption and theoretical studies, Lubricants 9 (2021) 93, https://doi.org/10.3390/lubricants9090093.
[105] X. Zhao, C. Chen, Q. Sun, Y. Li, H. Yu, Molecular structure optimization design of inhibitors based on frontier orbitals theory, Appl. Surf. Sci. 494 (2019) 895–907, https://doi.org/10.1016/j.apsusc.2019.07.248.
[106] A.A. Khadom, A.A. Mahmmod, Quantum chemical and mathematical statistical calculations of phenyltetrazole derivatives as corrosion inhibitors for mild steel in acidic solution: a theoretical approach, Results in Engineering 16 (2022) 100741, https://doi.org/10.1016/j.rineng.2022.100741.
[107] E.A. Erazua, B.B. Adeleke, A computational study of quinoline derivatives as corrosion inhibitors for mild steel in acidic medium, Jasem 23 (2019) 1819–1824, https://doi.org/10.4314/jasem.v23i10.8.
[108] B.T. Ogunyemi, D.F. Latona, A.A. Ayinde, I.A. Adejoro, Theoretical investigation to corrosion inhibition efficiency of some chloroquine derivatives using density functional theory, Adv. J. Chem. A 3 (2020) 485–492, https://doi.org/10.33945/SAMI/AJCA.2020.4.10.
[109] D.M. Mamand, T.M.K. Anwer, H.M. Qadr, Electronic structure and quantum chemical analysis of the corrosion inhibition efficiency of quinoxalines, J. Indian Chem. Soc. 100 (2023) 101018, https://doi.org/10.1016/j.jics.2023.101018.
[110] A. Chaouiki, F. Hazmatulhaq, D.I. Han, A.H. Al-Moubaraki, M. Bakhouch, Y.G. Ko, Predicting the interaction between organic layer and metal substrate through DFTB and electrochemical approach for excellent corrosion protection, J. Ind. Eng. Chem. 114 (2022) 190–204, https://doi.org/10.1016/j.jiec.2022.07.009.
[111] H. Lgaz, H. Lee, S. Kaya, R. Salghi, S.M. Ibrahim, M. Chafiq, L. Bazzi, Y.G. Ko, Unraveling bonding mechanisms and electronic structure of pyridine oximes on Fe(110) surface: deeper insights from DFT, molecular dynamics and SCC-DFT tight binding simulations, Molecules 28 (2023) 3545, https://doi.org/10.3390/molecules28083545.
[112] M. Murmu, S.Kr Saha, L. Guo, N.C. Murmu, P. Banerjee, Intrinsic electronic property and adsorption of organic molecules on specific iron surface: an *ab initio* DFT and DFTB study, J. Adhes. Sci. Technol. 37 (2023) 1837–1855, https://doi.org/10.1080/01694243.2022.2097580.
[113] H. Lgaz, H. Lee, Interfacial adsorption mechanism of hydroxycinnamic acids on iron surfaces: a computational perspective toward eco-friendly corrosion mitigation strategies, Appl. Surf. Sci. 644 (2024) 158763, https://doi.org/10.1016/j.apsusc.2023.158763.
[114] N.I.N. Haris, S. Sobri, Y.A. Yusof, N.K. Kassim, An overview of molecular dynamic simulation for corrosion inhibition of ferrous metals, Metals 11 (2020) 46, https://doi.org/10.3390/met11010046.
[115] L. Guo, S. Kaya, I.B. Obot, X. Zheng, Y. Qiang, Toward understanding the anticorrosive mechanism of some thiourea derivatives for carbon steel corrosion: a combined DFT and molecular dynamics investigation, J. Colloid Interface Sci. 506 (2017) 478–485, https://doi.org/10.1016/j.jcis.2017.07.082.
[116] C. Verma, H. Lgaz, D.K. Verma, E.E. Ebenso, I. Bahadur, M.A. Quraishi, Molecular dynamics and Monte Carlo simulations as powerful tools for study of interfacial adsorption behavior of corrosion inhibitors in aqueous phase: a review, J. Mol. Liq. 260 (2018) 99–120, https://doi.org/10.1016/j.molliq.2018.03.045.
[117] M. Beniken, R. Salim, E. Ech–chihbi, M. Sfaira, B. Hammouti, M. Ebn Touhami, M.A. Mohsin, M. Taleb, Adsorption behavior and corrosion inhibition mechanism of a polyacrylamide on C–steel in 0.5 M H2SO4: electrochemical assessments and molecular dynamic simulation, J. Mol. Liq. 348 (2022) 118022, https://doi.org/10.1016/j.molliq.2021.118022.
[118] A. Golchinvafa, S.H. Mousavi Anijdan, M. Sabzi, M. Sadeghi, The effect of natural inhibitor concentration of Fumaria officinalis and temperature on corrosion protection mechanism in API X80 pipeline steel in 1 M H2SO4 solution, Int. J. Pres. Ves. Pip. 188 (2020) 104241, https://doi.org/10.1016/j.ijpvp.2020.104241.
[119] U. Bharatiya, P. Gal, A. Agrawal, M. Shah, A. Sircar, Effect of corrosion on crude oil and natural gas pipeline with emphasis on prevention by ecofriendly corrosion inhibitors: a comprehensive review, J Bio Tribo Corros 5 (2019) 35, https://doi.org/10.1007/s40735-019-0225-9.
[120] S. Sharma, A. Kumar, Recent advances in metallic corrosion inhibition: a review, J. Mol. Liq. 322 (2021) 114862, https://doi.org/10.1016/j.molliq.2020.114862.
[121] A.A. Khadom, M.M. Kadhim, R.A. Anaee, H.B. Mahood, M.S. Mahdi, A.W. Salman, Theoritical evaluation of Citrus Aurantium leaf extract as green inhibitor for chemical and biological corrosion of mild steel in acidic solution: statistical, molecular dynamics, docking, and quantum mechanics study, J. Mol. Liq. 343 (2021) 116978, https://doi.org/10.1016/j.molliq.2021.116978.
[122] K. Adel, S.E. Hachani, I. Selatnia, N. Nebbache, S. Makhloufi, Correlating the inhibitory action of novel benzimidazole derivatives on mild steel corrosion with DFT-based reactivity descriptors and MD simulations, J. Indian Chem. Soc. 99 (2022) 100497, https://doi.org/10.1016/j.jics.2022.100497.